Smart Structures and Systems, *Vol. 29, No. 3 (2022) 395-420*
https://doi.org/10.12989/sss.2022.29.3.395

A new hybrid HSDT for bending, free vibration, and buckling analysis of FGM plates (2D & quasi-3D)

Y. Belkhodja [1,2], D. Ouinas*[1], H. Fekirini [2], J.A. Viña Olay [3], B. Achour [4], M. Touahmia [4] and M. Boukendakdji [4]

[1] *Laboratory of Science and Technology Environment and Valorization, Faculty of Sciences and Technology, Abdelhamid Ibn Badis University, Mostaganem 27000, Algeria*
[2] *Mechanics and physics of materials Laboratory, Mechanical Engineering Department, Faculty of Technology, Djillali Liabes University, Sidi Bel Abbes 22000, Algeria*
[3] *Materials Science and Metallurgical Engineering Department, University of Oviedo, Viesques Campus 33203, Gijón, Asturias, Spain*
[4] *Civil Engineering Department, University of Ha'il, KSA, Saudi Arabia*

(*Received April 29, 2020, Revised August 19, 2021, Accepted November 24, 2021*)

Abstract. A new hybrid quasi-3D and 2D high-order shear deformation theory is studied in this mathematical formulation, for an investigation of the bending, free vibrations and buckling influences on a functionally graded material plate. The theoretical formulation has been begun by a displacement field of five unknowns, governing the transverse displacement across the thickness of the plate by bending, shearing and stretching. The transverse shear deformation effect has been taken into consideration, satisfying the stress-free boundary conditions, especially on plate free surfaces as parabolic variation through its thickness. Thus, the mechanical properties of the functionally graded plate vary across the plate thickness, following three distributions forms: the power law, exponential form and the Mori-Tanaka scheme. The mechanical properties are used to develop the equations of motion, obtained from the Hamilton principle, and solved by applying the Navier-type solution for simply supported boundary conditions. The results obtained are compared with other solutions of 2D, 3D and quasi-3D plate theories have been found in the literature.

Keywords: bending; buckling; FGM plates; free vibration; HSDT-FGM; Quasi-3D and 2D theory; stretching effect

1. Introduction

Functionally graded materials (FGMs) are a new generation of composite materials (ceramic/metal), developed by a Japanese scientific group in 1984 (Koizumi 1997) for the purpose of an aerospace project that required thermal stress relaxation. FGMs have strongly proven their applications in the industrial sector and they have gained great popularity because of their considerable thermal and mechanical capabilities (Kawasaki and Watanabe 1988, Sasaki *et al*. 1989, Niino and Maeda 1990, Zhang *et al*. 2014, Barati and Shahverdi 2016, Darabi and Vosoughi 2016). These materials are used in harsh environments at high temperatures due to their ceramic-rich compositions, and can be subjected to extremely high thermal gradients, such as the case of aeronautical structures, space vehicles, nuclear enclosures ... etc. (Fukushima *et al*. 1990, Miyamoto *et al*. 1990, Sata *et al*. 1990, Shimoda *et al*. 1990, Yuki *et al*. 1990, Fukui 1991, Zhou *et al*. 2002, Zafarmand and Kadkhodayan 2015, Kolahchi *et al*. 2017). FGMs plates and shells are often used as structures in the engineering sector, to avoid problems of delamination and debonding, especially during dynamic and cyclic loadings. Many investigations were focused on the problems of buckling, bending and vibration based on different plate theories by using analytical and numerical solutions (Baferani *et al*. 2010, Arani *et al*. 2016, Kar and Panda 2016a, b, Raminnea *et al*. 2016). However, the theoretical formulations cited below are concerned with the analysis of bending, vibration as well as buckling. It has been developed in three phases, based on classical plate theory (CPT), first order transversal shear deformation (FSDT) theories, and the theory of high order transverse shear deformation (HSDT), which includes the effect of shear deformation without shear correction factor. Zenkour (2009) used a refined sinusoidal theory of plates for the analysis of thermos-elastic flexion of FGMs plates on two parameter foundations and subjected to transverse uniform loading. Aydogdu (2009) proposed a new higher order shear deformable laminated composite plate theory which is constructed from 3-D elasticity bending solutions by using an inverse method to study mechanical behavior laminated plates and beams. Benyoucef *et al*. (2010) investigated the static response of thick FGMs plates on Pasternak-type foundations using the hyperbolic theory of sheared formation, whereas Atmane *et al*. (2010) studied the dynamic response of FGMs plates. A Trigonometric Shear Deformation Theory (TSDT) for the static analysis of isotropic plate taking into account transverse shear deformation effect as well as transverse normal strain effect was presented by Ghugal and Sayyad (2010). Belabed *et al*.

*Corresponding author, Professor,
E-mail: douinas@gmail.com

ISSN: 1738-1584 (Print), 1738-1991 (Online)

(2014) presented the hyperbolic HSDT theory with stretching effect taking into account five unknowns in order to predict flexural and free vibrations responses of FGM plates. They indicated that the thickness stretching effect for thick plates was important. Iurlaro *et al*. (2014) used the Refined Zigzag Theory to study the bending and free vibration of sandwich plates embedding functionally graded layers. Several other studies on HSDT of FGM were performed, such as the theory of high order shear and normal deformations of a Plate (HOSNDPT) for which Qian *et al*. (2004) used the Petro-Galerkin Local No Mesh Method (MLPG) to study the flexion as well as the free and forced vibrations of a rectangular thick elastic FGM plate. They used the Mori-Tanaka homogenization technique to calculate the effective material properties.

A 3D free plate vibration analysis with FGM layers had also been studied by Hosseini-Hashemi *et al*. (2012), by assuming the Young's modulus and density exponentially variable over the plate thickness. Meshless global collocation method based on the thin plate spline radial basis function and *n*th-order shear deformation theory are used to analyze the free vibration of sandwich plate with functionally graded face and homogeneous core by Xiang *et al*. (2013). Tounsi and his collaborators *et al*. investigated FGM and composite mechanical responses using a new refined shear deformation theory (Beldjelili *et al*. 2016, Chikh *et al*. 2017, Zaoui *et al*. 2017, Bourada *et al*. 2012, Bouderba *et al*. 2013, Hebali *et al*. 2014, Zidi *et al*. 2014, Hanifi *et al*. 2017). A simple theory of sinusoidal shear deformation at four unknowns to analyze flexion, buckling and vibration of FGM plates was developed by Thai and Kim (2013). Kolahchi *et al*. (2016) analyzed the dynamic stability of temperature-dependent functionally graded CNT-reinforced visco-plates resting on orthotropic elastomeric medium. The theory of third order shear deformation (TSDT) was used with a non-meshed method by Ferreira *et al*. (2005), to analyze the bending problem, using a multi-quadric radial collocation function for FGMs plates with simply supported ends. Zenkour (2006) studied bending, using a generalized HSDT, for a square or rectangular FGMs plate with simply supported edges and subjected to a uniform transverse load. Matsunaga (2008) studied the natural frequencies and buckling stresses in a plate simply supported, taking into account the effect of transverse shear, normal deformations and rotational inertia. In this case, he used the power series expansion method for the displacement components in the dynamic equations for a 2D-HSDT. Madani *et al*. (2016) presented a differential cubature method for vibration analysis of embedded FG-CNT-reinforced piezoelectric cylindrical shells subjected to uniform and non-uniform temperature distributions. Talha and Singh (2010) used the HSDT theory to investigate the flexion and free vibrations of FGMs plates with different boundary conditions by introducing isoparametric finite elements with 13 degrees of freedom per node. Neves *et al*. (2011) studied the flexion of an FGM plate using the quasi-3D sinusoidal shear hybrid deformation theory. In this case, the equations of motion and the boundary conditions were obtained from the Carrera formulation (CUF). A new simple HSDT for bending and free vibration analysis of FGMs plate with simply supported edges was developed by Thai and Kim (2013). Arefi and Allam (2015) presented nonlinear analysis of an arbitrary functionally graded circular plate integrated with two functionally graded piezoelectric layers resting on the Winkler-Pasternak foundation. A new quasi-3D trigonometric HSDT with a new displacement field that introduces undetermined integral variables, have been developed by Abualnour *et al*. (2018), for free vibration analyses of FGMs plates with simply supported edges. Ameur *et al*. (2011) proposed a new theory of shear deformation to study the static response of FG plates on Pasternak-type elastic foundations. A nonlocal temperature-dependent dynamic buckling analysis of embedded sandwich micro plates reinforced by functionally graded carbon nanotubes (FG-CNTs) was presented by Shokravi and Jalili (2017). The quasi-3D SSDT theory as well as a new application of CUF in the free flexion and vibration analysis of FGMs plates, was proposed by Neves *et al*. (2012a), where motion equations were interpolated by radial basis functions collocation. Another theory, quasi-3D hyperbolic sinusoidal HSDT was developed by Neves *et al*. (2012b), to obtain motion equations and boundary conditions when combined with the non-mesh technique. Chen (2018) presented a numerical solution for the thick cylinders made of functionally graded materials (FGMs) with a constant Poisson\'s ratio and an arbitrary Young's modulus using transfer matrix method. Zaoui *et al*. (2019) proposed a new 2D and quasi-3D theory capable of modeling the dynamic behavior of FGM plates on elastic foundations using a new shear deformation form function. Xiang and Kang (2013) studied the natural frequencies of FGM plates on elastic foundations using n-th order shear deformation theory as well as a non-mesh approach. The proposed theory is a generalization of Reddy's third-order shear deformation theory (Reddy, 2000). the buckling, and free vibration analysis of tapered functionally graded carbon nanotube reinforced composite (FG-CNTRC) micro Reddy beam under longitudinal magnetic field using finite element method (FEM) is investigated by Mohammadimehr and Alimirzaei (2017). Porosities effects on the bending response of functionally graded material (FGM) sandwich plates were analyzed by Daikh and Zenkour (2019). Mantari and Soares (2013) developed a new quasi-3D trigonometric HSDT for the static response analysis of FGMs plates subjected to bi-sinusoidal loading in the presence of the stretching effect. This work had been expanded for a doubly-curved shell (Mantari and Soares 2014). An analytical solution of the equations governing the static response of a thick FGM plate with simply supported edges, subjected to a bi-sinusoidal transverse load using a new trigonometric HSDT theory was developed by Mantari and Soares (2012a) whereas Mantari and Soares (2012b) solved the same problem using the generalized quasi-3D hybrid theory of deformation HSDT. Belkhodja *et al*. (2019) studied the flexion, free vibrations and buckling of FGMs plate with simply supported edges using the exponential-trigonometric shear function. Mahesh *et al*. (2019) studied the coupled free vibration problem of skew magneto-electro-elastic plates (SMEE) considering the temperature-moisture

dependent material properties in which the plate kinematics follows Reddy's higher order shear deformation theory. Amir *et al*. (2020) analyzed size-dependent free vibration of three-layered FG porous micro rectangular plate integrated by nano-composite faces in hygrothermal environment using a quasi-3D tangential shear deformation theory. Le *et al*. (2020) developed finite element formulations for evaluating vibration characteristics of FGSW plates partially supported by Pasternak foundation based on a refined third-order shear deformation theory. Free axisymmetric vibrations of functionally graded circular plates subjected to a non-linear temperature distribution along the thickness direction have been studied on the basis of classical plate theory by Lal and Saini (2020). A new quasi-3D trigonometric HSDTs with a new displacement field with undetermined integral variables, had been developed for analyzing bending and free vibrations of FGMs plates with simply supported edges (Hebbar *et al*. 2020, Zaoui *et al*. 2020).

In this paper, a new high order shear deformation theory with five unknowns is developed for FGM plates with the presence of stretching effect. Bending, free vibration and buckling are investigated using a new quasi-3D and 2D hybrid (polynomial-hyperbolic-exponential) HSDT of simply supported square or rectangular plates. The displacement field is chosen as a function of a new polynomial-hyperbolic-exponential variation form of displacements on the transverse planes through the thickness with no tangential stresses on the edge of the plate surfaces. The Hamilton principle is used to derive motion equations and the Navier-type analytical solutions for simply supported plates which are compared to existing solutions to verify the validity of the developed theory. The properties of the material vary continuously through the thickness of the plate by the power law, the exponential form and the Mori-Tanaka scheme. The effects of the material index (power index) and length/width, length/thickness ratios on deflection, normal and shear stresses, critical buckling load and natural frequencies are highlighted. The numerical results are presented and compared with the solutions from the literature, to check the accuracy and efficiency of the current theory.

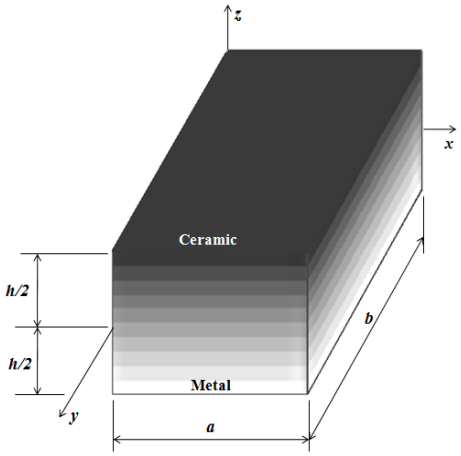

Fig. 1 The FGMs plate geometric model

2. Theoretical formulation

The consideration of transverse shear in the study of functionally graded materials has proven to be preponderant for obtaining consistent and exploitable results, both analytically and numerically. In the present study, the system of equations governing the FGMs plate is determined using the variation approach method. The origin of the material coordinates is taken at the center of the plate on the middle plane (x, y, 0), as shown in Fig. 1. For a precise analysis of transverse shear effects in the mathematical model, the HSDT model has been used with three components: bending w_b, shearing w_s and stretching w_{st} as functions of x, y coordinates and time t. Moreover, the normal transversal stress is negligible compared to the plane stresses σ_x and σ_y.

2.1 The design and analytical formulation

In this paper, a plate of the following dimensions is considered: length (a), width (b) and uniform thickness (h), as shown in Fig. 2. The change in thickness follows the z coordinate (z axis) perpendicular to the middle plane (x, y) of the plate. Two geometric ratios are defined by the

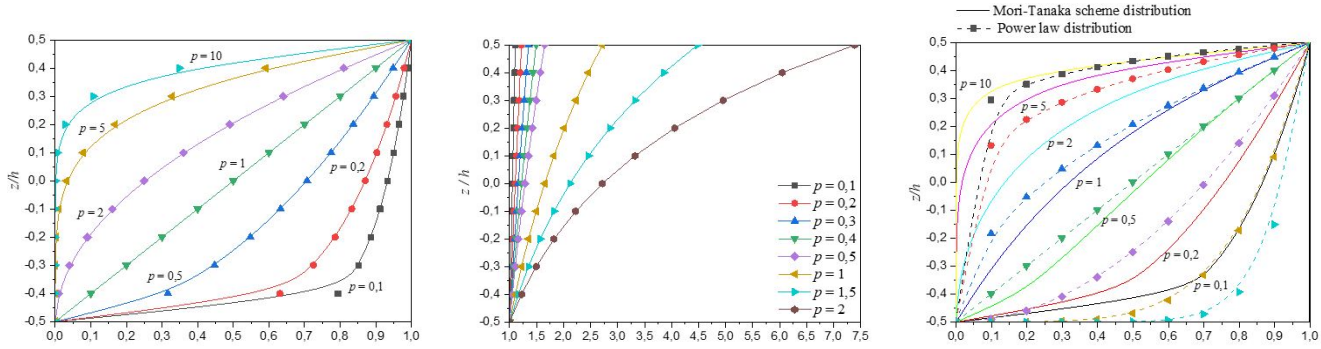

(a) V_c (b) V_{c1} (c) V_{c2}

Fig. 2 Ceramic material volume fraction: (a) Power law function profile $V_c\,(z) = (z/h + 0.5)^P$ along the thickness of P-FGM plate; (b) Exponential function profile $V_{c1}(z) = e^{P\left(\frac{z}{h}+0.5\right)} = e^{P\left(\sqrt[P]{V_c(z)}\right)}$ along the thickness of E-FGM plate; (c) Mori-Tanaka scheme function profile $V_{c2}(z) = V_c(z)$. $[(3-3v)/\left[(3-3v)+\left(1-V_c(z)\right)[(E_c-E_m)-1](1+v)\right]]$ along the thickness of MT-FGM plate

Table 1 Material properties of metal and ceramics

Materials		Material properties		
		Young's modulus (GPa)	Mass density (kg/m^3)	Poisson's ratio
Metal	Aluminium (Al)	70	2702	0.3
Ceramic	Zirconia (ZrO_2)	200	5700	0.3
	Alumina (Al_2O_3)	380	3800	0.3

dimensions of the plate: The ratio length/thickness (a/h), and ratio length/width (a/b). It is known that the thickness of the plate varies proportionally with the transverse shear deformation effects, therefore the ratios (a/h) characterize three forms of plate: a thick plate with a low ratio (a/h), moderately thick plate ($a/h \approx 10$), a thin plate with a large ratio (a/h). Moreover, the ratios ($a/b = 1$) and ($a/b \neq 1$) define a square and a rectangular plate respectively. For various structural and functional uses, FGMs can be applied to different pairs of materials. However, the plate currently under study is made in the form of a mixture of two different materials, a metal (Aluminum: Al) and a ceramic (Alumina: Al_2O_3 or Zirconia: ZrO_2). The mechanical properties are summarized in Table 1. The continuous gradation of the mixture of pairs of materials depends on the position (z) of the plate thickness and the effective mechanical properties. The later depend on a volume fraction as a function of the index (p).

2.2 Effective mechanical properties of FGM plates

FGMs are heterogeneous and idealized, their mechanical properties change regularly with respect to coordinates in the plane (Nguyen 2014). Its composition and structure change gradually, resulting in a corresponding modification of the effective mechanical properties of the material, namely the Young's modulus, the Poisson's ratio and the density (Koizumi 1997). These properties are supposed to be classified by a simple continuous and non-discrete model, when the microstructure is neglected and the distribution continues through the thickness of the plate (z axes) is taken into account. The effective mechanical properties are described from the homogeneous plate theories, after homogenization of the FGMs plate with their effective modules (Reddy 2000).

2.2.1 Young's modulus

Only the Young's modulus follows three mathematical formulations, the first is the power law (Zenkour 2007, Kiran and Kattimani 2018), the second is the exponential form (Tornabene 2009, Celebi *et al*. 2016) and the third is the Mori-Tanaka scheme (Younsi *et al*. 2018) respectively according to the following Eqs. (1a), (1b) and (1c)

$$E(z) = (E_c - E_m)V_c(z) + E_m \tag{1a}$$

$$E(z) = E_c V_{c1}(z), \qquad p \in]0, \infty[\tag{1b}$$

$$E(z) = (E_c - E_m)V_{c2}(z) + E_m \tag{1c}$$

Where E_c and E_m are Young's moduli of the upper (ceramic) and lower (metal) faces of the plate respectively. V_c, V_{c1} and V_{c2} represent the volume fractions of the ceramic material, defined by the Eqs. (2a), (2b) and (2c), respectively

$$V_c(z) = \left(\frac{1}{2} + \frac{z}{h}\right)^P, \tag{2a}$$

$$V_{c1}(z) = e^{p\left(\sqrt[p]{V_c(z)}\right)} \tag{2b}$$

$$V_{c2}(z) = \frac{(3-3\nu)V_c(z)}{(3-3\nu) + (1-V_c(z))(E_c/E_m - 1)(1+\nu)} \tag{2c}$$

where p is a positive volume fraction index given for three types of plate. The first is a homogeneous ceramic plate (p = 0, extremely rigid), the second is a FGM plate $p \in]0, \infty[$ (from the most rigid to the most ductile FGM) and the metal plate ($p \to \infty$, very ductile). The index p specifies three FGMs profile distributions over the plate thickness $z \in]-h/2, h/2[$, following the fraction of volume V_c, V_{c1} and V_{c2} as shown in Figs. 2(a), (b) and (c), respectively.

2.2.2 Poisson's ratio

When the Poisson coefficients $\nu(z)$ of the ceramic and the metal are almost identical, then the results of two homogenization techniques are close to each other (Jha *et al*. 2012). As a result, the Poisson's ratio is considered constant because there is no significant difference between the results obtained and it has no significant effect on the FGM plate (Ferreira 2005, Vaghefi *et al*. 2010).

2.2.3 The volume mass or density

The effective density $\rho(z)$ is estimated using the power law distribution with the rule of Voigt mixtures (Mantari *et al*. 2012, Guerroudj *et al*. 2018) as

$$\rho(z) = (\rho_c - \rho_m)V_c(z) + \rho_m \tag{3}$$

2.3 Kinematics, deformation, stresses and energy

2.3.1 Kinematics

The present HSDT formulation follows the development procedure of Thai and Kim (2013) and Belabed *et al*. (2014), initiated by a transverse displacement field along (z) and accounts for three different displacements: bending (w_b), shearing (w_s) and stretching (w_{st}) through the thickness of the plate, with five unknowns only. The displacements are considered small compared to the thickness of the plate and, consequently, the deformations are infinitesimal. A new function of form $f(z)$ is used to characterize the evolution of transverse shear deformation. The displacement field is written as Eqs. (4a), (4b) and (4c)

$$u(x,y,z,t) = u_0(x,y,t) - z\frac{\partial w_b}{\partial x} - f(z)\frac{\partial w_s}{\partial x} \quad (4a)$$

$$v(x,y,z,t) = v_0(x,y,t) - z\frac{\partial w_b}{\partial y} - f(z)\frac{\partial w_s}{\partial y} \quad (4b)$$

$$w(x,y,z,t) = w_b(x,y,t) + w_s(x,y,t) + w_{st}(x,y,t) \quad (4c)$$

where u_0 and v_0 are respectively the displacements on the x and y coordinate axes on the plate mid-plane. w_{st} is defined for 2D HSDT $(\varepsilon_z = 0)$ as

$$w_{st}(x,y,t) = 0 \quad (5a)$$

Therefore, for 3D and quasi-3D HSDT $(\varepsilon_z \neq 0)$, it is defined as

$$w_{st}(x,y,t) = g(z)\phi(x,y,t) \quad (5b)$$

where φ is an additional component of transverse displacement which takes into account the effect of normal stress (stretching effect). $f(z)$ defines the transverse shear deformation effect across the thickness (h). Several models of shape functions have been suggested by the researchers, and in this study, a new hybrid function is developed from the polynomial, exponential and hyperbolic functions. It is presented in the equation below (6)

$$f(z) = z \cdot \left(\left(\frac{25z^2}{\pi\left(z^2 h + h^3\right)} + cosh\left(\frac{\pi z}{h}\right) + e^{\frac{z^2}{h^2}} \right) - 11.188117 \right) \quad (6)$$

$$g(z) = 1 - \frac{df(z)}{dz}, \quad (7)$$

2.3.2 Deformations

The application of the linear elasticity theory based on the derivative of the displacement field of Eq. (4) gives rise to the following linear deformation field

$$\begin{Bmatrix} \varepsilon_x \\ \varepsilon_y \\ \varepsilon_z \\ \gamma_{yz} \\ \gamma_{xz} \\ \gamma_{xy} \end{Bmatrix} = \begin{Bmatrix} \frac{\partial u_0}{\partial x} \\ \frac{\partial v_0}{\partial y} \\ 0 \\ 0 \\ 0 \\ \frac{\partial u_0}{\partial y} + \frac{\partial v_0}{\partial x} \end{Bmatrix} - z \begin{Bmatrix} \frac{\partial^2 w_b}{\partial x^2} \\ \frac{\partial^2 w_b}{\partial y^2} \\ 0 \\ 0 \\ 0 \\ 2\frac{\partial^2 w_b}{\partial x \partial y} \end{Bmatrix} - \begin{Bmatrix} f(z)\frac{\partial^2 w_s}{\partial x^2} \\ f(z)\frac{\partial^2 w_s}{\partial y^2} \\ -g'(z)\ \phi \\ -g(z)\left(\frac{\partial w_s}{\partial y} + \frac{\partial \phi}{\partial y}\right) \\ -g(z)\left(\frac{\partial w_s}{\partial x} + \frac{\partial \phi}{\partial x}\right) \\ 2f(z)\frac{\partial^2 w_s}{\partial x \partial y} \end{Bmatrix} \quad (8)$$

and

$$g'(z) = \frac{dg(z)}{dz} = \frac{d^2 f(z)}{dz^2} \quad (9)$$

2.3.3 Stresses

The relations constituting the linear behavior of FGMs plate are rewritten in terms of the rigidity matrix as follows

$$\begin{Bmatrix} \sigma_x \\ \sigma_y \\ \sigma_z \\ \tau_{yz} \\ \tau_{xz} \\ \tau_{xy} \end{Bmatrix} = \begin{bmatrix} C_{11} & C_{12} & C_{13} & 0 & 0 & 0 \\ C_{12} & C_{22} & C_{23} & 0 & 0 & 0 \\ C_{13} & C_{23} & C_{33} & 0 & 0 & 0 \\ 0 & 0 & 0 & C_{44} & 0 & 0 \\ 0 & 0 & 0 & 0 & C_{55} & 0 \\ 0 & 0 & 0 & 0 & 0 & C_{66} \end{bmatrix} \begin{Bmatrix} \varepsilon_x \\ \varepsilon_y \\ \varepsilon_z \\ \gamma_{yz} \\ \gamma_{xz} \\ \gamma_{xy} \end{Bmatrix} \quad (10)$$

where the rigidity coefficients defined for 2D HSDT $(\varepsilon_z = 0)$ are given by

$$C_{11} = C_{22} = \frac{E(z)}{1-\nu^2}, \quad (11a)$$

$$C_{12} = \nu C_{11}, \qquad C_{13} = C_{23} = 0, \quad (11b)$$

$$C_{44} = C_{55} = C_{66} = \frac{E(z)}{2(1+\nu)} \quad (11c)$$

And therefore, for 3D and quasi-3D HSDT $(\varepsilon_z \neq 0)$ are

$$C_{11} = C_{22} = C_{33} = \frac{(1-\nu)E(z)}{(1-2\nu)(1+\nu)}, \quad (12a)$$

$$C_{12} = C_{13} = C_{23} = \frac{\nu E(z)}{(1-2\nu)(1+\nu)}, \quad (12b)$$

$$C_{44} = C_{55} = C_{66} = \frac{E(z)}{2(1+\nu)} \quad (12c)$$

2.3.4 Energy principle

To determine the equations of motion of a deformable solid, the Hamilton principle is used (Meftah *et al*. 2017, Singh and Panda 2015). The principle can be formulated

analytically in the following form

$$0 = \int_0^{t'} (\delta U + \delta V - \delta K)\, dt \qquad (13)$$

where t' denotes a period of time and δU, δV and δK are, respectively, the strain energy variation, the work done by the external loadings and the kinetic energy of the FGMs plate.

2.3.4.1 Deformation energy Work done by external loadings

The variation of the strain energy is calculated below as follows

$$\delta\, U = \int_V (\sigma_x \delta\, \varepsilon_x + \sigma_y \delta\, \varepsilon_y + \sigma_z \delta\, \varepsilon_z + \tau_{xy} \delta\, \gamma_{xy} + \tau_{yz} \delta\, \gamma_{yz} + \tau_{xz} \delta\, \gamma_{xz})\, dV \qquad (14a)$$

$$\begin{aligned} \delta\, U = \int_A \Big[& N_x \frac{\partial \delta u_0}{\partial x} - M_x^b \frac{\partial^2 \delta w_b}{\partial x^2} - M_x^s \frac{\partial^2 \delta w_s}{\partial x^2} + N_y \frac{\partial \delta v_0}{\partial y} - M_y^b \frac{\partial^2 \delta w_b}{\partial y^2} - M_y^s \frac{\partial^2 \delta w_s}{\partial y^2} + N_{xy} \left(\frac{\partial \delta u_0}{\partial y} + \frac{\partial \delta v_0}{\partial x} \right) \\ & -2M_{xy}^b \frac{\partial^2 \delta w_b}{\partial x \partial y} - 2M_{xy}^s \frac{\partial^2 \delta w_s}{\partial x \partial y} + S_{xz}^s \left(\frac{\partial \delta w_s}{\partial x} + \frac{\partial \delta \phi}{\partial x} \right) + S_{yz}^s \left(\frac{\partial \delta w_s}{\partial y} + \frac{\partial \delta \phi}{\partial y} \right) - N_z\, \delta \phi \Big] dA \end{aligned} \qquad (14b)$$

where A, N, M and S denote respectively the section, the volume and the stress resultants defined as follows

$$\begin{bmatrix} N_x & N_y & 0 & 0 & 0 & N_{xy} \\ M_x^b & M_y^b & 0 & 0 & 0 & M_{xy}^b \\ M_x^s & M_y^s & 0 & 0 & 0 & M_{xy}^s \\ 0 & 0 & 0 & S_{yz}^s & S_{xz}^s & 0 \\ 0 & 0 & N_z & 0 & 0 & 0 \end{bmatrix} = \int_{-h/2}^{h/2} \begin{Bmatrix} 1 \\ z \\ f(z) \\ g(z) \\ g'(z) \end{Bmatrix} \{\sigma_x \quad \sigma_y \quad \sigma_z \quad \tau_{yz} \quad \tau_{xz} \quad \tau_{xy}\}\, dz \qquad (15)$$

2.3.4.2 Work done by external loadings

The variation of the potential energy of the external loads in the horizontal and transverse directions can be expressed by

$$\delta V = -\int_A (N + q)\delta(w_b + w_s + w_{st})\, dA \qquad (16)$$

where N is a compressive in plane load. It is assumed that the plate is subjected to this load in two directions, as shown below

$$N = N_x^0 \frac{\partial^2 w_0}{\partial x^2} + 2N_{xy}^0 \frac{\partial^2 w_0}{\partial x \partial y} + N_y^0 \frac{\partial^2 w_0}{\partial y^2} \qquad (17)$$

where $N_x^0 = -N_0$, $N_y^0 = -\gamma$, $N_{xy}^0 = 0$ and γ is the dimensionless load parameter, defining three types of in-plane loads such as axial compressive-tensile load ($\gamma = 0$), uni-axial compression load ($\gamma = 1$) and a bi-axial compressive load ($\gamma = -1$) and q is the mechanical transverse sinusoidal load, parallel to the transverse direction of the plate.

2.3.4.3 The kinetic energy

The variation of the kinetic energy can be calculated by

$$\delta K = \int_{-h/2}^{h/2} \int_A (\dot{u}\delta\dot{u} + \dot{v}\delta\dot{v} + \dot{w}\delta\dot{w})\, \rho(z) dA \qquad (18a)$$

$$\begin{aligned} \delta K = \int_A \Big[& I_0 \big(\dot{u}_0 \delta\dot{u}_0 + \dot{v}_0 \delta\dot{v}_0 + (\dot{w}_b + \dot{w}_s)(\delta\dot{w}_b + \delta\dot{w}_s) \big) - I_1 \left(\dot{u}_0 \frac{\partial \delta\dot{w}_b}{\partial x} + \frac{\partial \dot{w}_b}{\partial x} \delta\dot{u}_0 + \dot{v}_0 \frac{\partial \delta\dot{w}_b}{\partial y} + \frac{\partial \dot{w}_b}{\partial y} \delta\dot{v}_{.0} \right) \\ & + I_2 \left(\frac{\partial \dot{w}_b}{\partial x} \frac{\partial \delta\dot{w}_b}{\partial x} + \frac{\partial \dot{w}_b}{\partial y} \frac{\partial \delta\dot{w}_b}{\partial y} \right) - J_1 \left(\dot{u}_0 \frac{\partial \delta\dot{w}_s}{\partial x} + \frac{\partial \dot{w}_s}{\partial x} \delta\dot{u}_0 + \dot{v}_0 \frac{\partial \delta\dot{w}_s}{\partial y} + \frac{\partial \dot{w}_s}{\partial y} \delta\dot{v}_{.0} \right) \\ & + J_2 \left(\frac{\partial \dot{w}_b}{\partial x} \frac{\partial \delta\dot{w}_s}{\partial x} + \frac{\partial \dot{w}_s}{\partial x} \frac{\partial \delta\dot{w}_b}{\partial x} + \frac{\partial \dot{w}_b}{\partial y} \frac{\partial \delta\dot{w}_s}{\partial y} + \frac{\partial \dot{w}_s}{\partial y} \frac{\partial \delta\dot{w}_b}{\partial y} \right) + K_2 \left(\frac{\partial \dot{w}_s}{\partial x} \frac{\partial \delta\dot{w}_s}{\partial x} + \frac{\partial \dot{w}_s}{\partial y} \frac{\partial \delta\dot{w}_s}{\partial y} \right) \\ & + J_1^s \left((\dot{w}_b + \dot{w}_s)\delta\dot{\phi} + \dot{\phi}.\delta(\dot{w}_b + \dot{w}_s) \right) + K_2^s \dot{\phi}.\delta\dot{\phi} \Big] dA dz \end{aligned} \qquad (18b)$$

where by convention, the dots express the derivative with respect to time (t). The terms I_i, J_i and K_i denote the inertia moments expressed by

$$(I_0, I_1, I_2, J_1, J_2, K_2, J_1^s, K_2^s) = \int_{-h/2}^{h/2} \rho(z)[1, z, z^2, f(z), zf(z), f^2(z), g(z), g^2(z)]dz \tag{19}$$

2.4 The equations of motion

The motion equations appropriate to the five unknowns of the displacement field are obtained by substituting the energy Eqs. (14), (16) and (18) in Eq. (13). By regrouping all the coefficients $\delta u_0, \delta v_0, \delta w_0$ and $\delta\phi$ after integration by part, the system of equations can be written as follows

$$\delta u_0: \quad \frac{\partial N_x}{\partial x} + \frac{\partial N_{xy}}{\partial y} = I_0\ddot{u}_0 - I_1\frac{\partial \ddot{w}_b}{\partial x} - J_1\frac{\partial \ddot{w}_s}{\partial x} \tag{20a}$$

$$\delta v_0: \quad \frac{\partial N_{xy}}{\partial x} + \frac{\partial N_y}{\partial y} = I_0\ddot{v}_0 - I_1\frac{\partial \ddot{w}_b}{\partial y} - J_1\frac{\partial \ddot{w}_s}{\partial y} \tag{20b}$$

$$\delta w_b: \quad \frac{\partial^2 M_x^b}{\partial x^2} + 2\frac{\partial^2 M_{xy}^b}{\partial x \partial y} + \frac{\partial^2 M_y^b}{\partial y^2} + q = I_0(\ddot{w}_b + \ddot{w}_s) + I_1\left(\frac{\partial \ddot{u}_0}{\partial x} + \frac{\partial \ddot{v}_0}{\partial y}\right) - I_2\nabla^2\ddot{w}_b - J_2\nabla^2\ddot{w}_s + J_1^s\ddot{\phi} \tag{20c}$$

$$\delta w_s: \quad \frac{\partial^2 M_x^s}{\partial x^2} + 2\frac{\partial^2 M_{xy}^s}{\partial x \partial y} + \frac{\partial^2 M_y^s}{\partial y^2} + \frac{\partial S_{xz}^s}{\partial x} + \frac{\partial S_{yz}^s}{\partial y} + q = I_0(\ddot{w}_b + \ddot{w}_s) + J_1\left(\frac{\partial \ddot{u}_0}{\partial x} + \frac{\partial \ddot{v}_0}{\partial y}\right) - J_2\nabla^2\ddot{w}_b - K_2\nabla^2\ddot{w}_s + J_1^s\ddot{\phi} \tag{20d}$$

$$\delta\phi: \quad \frac{\partial S_{xz}^s}{\partial x} + \frac{\partial S_{yz}^s}{\partial y} - N_z = J_1^s(\ddot{w}_b + \ddot{w}_s) + K_2^s\ddot{\phi} \tag{20e}$$

Where ∇^2 is the Laplacian operator. The resulting stresses are obtained by substituting Eq. (10) in (15), giving (21)

$$\begin{Bmatrix} N_x \\ N_y \\ N_{xy} \\ M_x^b \\ M_y^b \\ M_{xy}^b \\ M_x^s \\ M_y^s \\ M_{xy}^s \\ S_{yz}^s \\ S_{xz}^s \\ N_z \end{Bmatrix} = \begin{bmatrix} A_{11} & A_{12} & 0 & B_{11} & B_{12} & 0 & B_{11}^s & B_{12}^s & 0 & 0 & 0 & P \\ A_{12} & A_{22} & 0 & B_{12} & B_{22} & 0 & B_{12}^s & B_{22}^s & 0 & 0 & 0 & P \\ 0 & 0 & A_{66} & 0 & 0 & B_{66} & 0 & 0 & B_{66}^s & 0 & 0 & 0 \\ B_{11} & B_{12} & 0 & D_{11} & D_{12} & 0 & D_{11}^s & D_{12}^s & 0 & 0 & 0 & P^a \\ B_{12} & B_{22} & 0 & D_{12} & D_{22} & 0 & D_{12}^s & D_{22}^s & 0 & 0 & 0 & P^a \\ 0 & 0 & B_{66} & 0 & 0 & D_{66} & 0 & 0 & D_{66}^s & 0 & 0 & 0 \\ B_{11}^s & B_{12}^s & 0 & D_{11}^s & D_{12}^s & 0 & H_{11}^s & H_{12}^s & 0 & 0 & 0 & T \\ B_{12}^s & B_{22}^s & 0 & D_{12}^s & D_{22}^s & 0 & H_{12}^s & H_{22}^s & 0 & 0 & 0 & T \\ 0 & 0 & B_{66}^s & 0 & 0 & D_{66}^s & 0 & 0 & H_{66}^s & 0 & 0 & 0 \\ 0 & 0 & 0 & 0 & 0 & 0 & 0 & 0 & 0 & A_{44}^s & 0 & 0 \\ 0 & 0 & 0 & 0 & 0 & 0 & 0 & 0 & 0 & 0 & A_{55}^s & 0 \\ P & P & 0 & P^a & P^a & 0 & T & T & 0 & 0 & 0 & T^a \end{bmatrix} \begin{Bmatrix} \frac{\partial u_0}{\partial x} \\ \frac{\partial v_0}{\partial y} \\ \frac{\partial u_0}{\partial y} + \frac{\partial v_0}{\partial x} \\ -\frac{\partial^2 w_b}{\partial x^2} \\ -\frac{\partial^2 w_b}{\partial y^2} \\ -2\frac{\partial^2 w_b}{\partial x \partial y} \\ -\frac{\partial^2 w_s}{\partial x^2} \\ -\frac{\partial^2 w_s}{\partial y^2} \\ -2\frac{\partial^2 w_s}{\partial x \partial y} \\ \left(\frac{\partial w_s}{\partial y} + \frac{\partial \phi}{\partial y}\right) \\ \left(\frac{\partial w_s}{\partial x} + \frac{\partial \phi}{\partial x}\right) \\ \phi \end{Bmatrix} \tag{21}$$

Where for quasi-3D HSDT ($\varepsilon_z \neq 0$), the rigidity coefficients are written

$$(A, B, D, B^s, D^s, H^s, A^s) = \int_{-h/2}^{h/2} [1, z, z^2, f(z), zf(z), f^2(z), g^2(z)] \cdot Q(z)dz \tag{22a}$$

$$\begin{Bmatrix} A_{11} & B_{11} & D_{11} & B_{11}^s & D_{11}^s & H_{11}^s \\ A_{12} & B_{12} & D_{12} & B_{12}^s & D_{12}^s & H_{12}^s \\ A_{66} & B_{66} & D_{66} & B_{66}^s & D_{66}^s & H_{66}^s \end{Bmatrix} = \int_{-h/2}^{h/2} (1, z, z^2, f(z), zf(z), [f(z)]^2) \begin{Bmatrix} C_{11}(z) \\ C_{12}(z) \\ G(z) \end{Bmatrix} dz, \tag{22b}$$

$$(A_{22}, B_{22}, D_{22}, B_{22}^s, D_{22}^s, H_{22}^s) = (A_{11}, B_{11}, D_{11}, B_{11}^s, D_{11}^s, H_{11}^s) \tag{22c}$$

$$A_{44}^s = A_{55}^s = \int_{-h/2}^{h/2} [g(z)]^2 G(z) dz \tag{22d}$$

$$\{P, \quad P^a, \quad T, \quad T^a\} = \int_{-h/2}^{h/2} (g'(z), zg'(z), f(z)g'(z), [g'(z)]^2) C_{11}(z)\, dz \tag{22e}$$

The equations of motion (20) can be expressed in terms of displacement using the system of Eq. (21), giving

$$\begin{aligned} \delta u_0: \; & A_{11}\frac{\partial^2 u_0}{\partial x^2} + A_{66}\frac{\partial^2 u_0}{\partial y^2} + (A_{12}+A_{66})\frac{\partial^2 v_0}{\partial x \partial y} - B_{11}\frac{\partial^3 w_b}{\partial x^3} - (B_{12}+2B_{66})\frac{\partial^3 w_b}{\partial x \partial y^2} - B_{11}^s\frac{\partial^3 w_s}{\partial x^3} \\ & -(B_{12}^s+2B_{66}^s)\frac{\partial^3 w_s}{\partial x \partial y^2} + P\frac{\partial \phi}{\partial x} = I_0\ddot{u}_0 - I_1\frac{\partial \ddot{w}_b}{\partial x} - J_1\frac{\partial \ddot{w}_s}{\partial x} \end{aligned} \tag{23a}$$

$$\begin{aligned} \delta v_0: \; & A_{22}\frac{\partial^2 v_0}{\partial y^2} + A_{66}\frac{\partial^2 v_0}{\partial x^2} + (A_{12}+A_{66})\frac{\partial^2 u_0}{\partial x \partial y} - B_{22}\frac{\partial^3 w_b}{\partial y^3} - (B_{12}+2B_{66})\frac{\partial^3 w_b}{\partial x^2 \partial y} - B_{22}^s\frac{\partial^3 w_s}{\partial y^3} \\ & -(B_{12}^s+2B_{66}^s)\frac{\partial^3 w_s}{\partial x^2 \partial y} + P\frac{\partial \phi}{\partial y} = I_0\ddot{v}_0 - I_1\frac{\partial \ddot{w}_b}{\partial y} - J_1\frac{\partial \ddot{w}_s}{\partial y} \end{aligned} \tag{23b}$$

$$\begin{aligned} \delta w_b: \; & B_{11}\frac{\partial^3 u_0}{\partial x^3} + (B_{12}+2B_{66})\frac{\partial^3 u_0}{\partial x \partial y^2} + (B_{12}+2B_{66})\frac{\partial^3 v_0}{\partial x^2 \partial y} - B_{22}\frac{\partial^3 v_0}{\partial y^3} - D_{11}\frac{\partial^4 w_b}{\partial x^4} - D_{22}\frac{\partial^4 w_b}{\partial y^4} \\ & -2(D_{12}+2D_{66})\frac{\partial^4 w_b}{\partial x^2 \partial y^2} - D_{11}^s\frac{\partial^4 w_s}{\partial x^4} - D_{22}^s\frac{\partial^4 w_s}{\partial y^4} - 2(D_{12}^s+2D_{66}^s)\frac{\partial^4 w_s}{\partial x^2 \partial y^2} + P^a\left(\frac{\partial^2 \phi}{\partial x^2}+\frac{\partial^2 \phi}{\partial y^2}\right) + q \\ & = I_0(\ddot{w}_b+\ddot{w}_s) + I_1\left(\frac{\partial \ddot{u}_0}{\partial x}+\frac{\partial \ddot{v}_0}{\partial y}\right) - I_2\left(\frac{\partial^2 \ddot{w}_b}{\partial^2 x}+\frac{\partial^2 \ddot{w}_b}{\partial^2 y}\right) - J_2\left(\frac{\partial^2 \ddot{w}_s}{\partial^2 x}+\frac{\partial^2 \ddot{w}_s}{\partial^2 y}\right) + J_1^s\ddot{\phi} \end{aligned} \tag{23c}$$

$$\begin{aligned} \delta w_s: \; & B_{11}^s\frac{\partial^3 u_0}{\partial x^3} + (B_{12}^s+2B_{66}^s)\frac{\partial^3 u_0}{\partial x \partial y^2} + (B_{12}^s+2B_{66}^s)\frac{\partial^3 v_0}{\partial x^2 \partial y} + B_{22}^s\frac{\partial^3 v_0}{\partial y^3} - D_{11}^s\frac{\partial^4 w_b}{\partial x^4} - D_{22}^s\frac{\partial^4 w_b}{\partial y^4} \\ & -2(D_{12}^s+2D_{66}^s)\frac{\partial^4 w_b}{\partial x^2 \partial y^2} + A_{44}^s\frac{\partial^2 w_s}{\partial y^2} + A_{55}^s\frac{\partial^2 w_s}{\partial x^2} - H_{11}^s\frac{\partial^4 w_s}{\partial x^4} - 2(H_{12}^s+2H_{66}^s)\frac{\partial^4 w_s}{\partial x^2 \partial y^2} \\ & -H_{22}^s\frac{\partial^4 w_s}{\partial y^4} + T\left(\frac{\partial^2 \phi}{\partial x^2}+\frac{\partial^2 \phi}{\partial y^2}\right) + A_{44}^s\frac{\partial^2 \phi}{\partial y^2} + A_{55}^s\frac{\partial^2 \phi}{\partial x^2} + q \\ & = I_0(\ddot{w}_b+\ddot{w}_s) + J_1\left(\frac{\partial \ddot{u}_0}{\partial x}+\frac{\partial \ddot{v}_0}{\partial y}\right) - J_2\left(\frac{\partial^2 \ddot{w}_b}{\partial^2 x}+\frac{\partial^2 \ddot{w}_b}{\partial^2 y}\right) - K_2\left(\frac{\partial^2 \ddot{w}_s}{\partial^2 x}+\frac{\partial^2 \ddot{w}_s}{\partial^2 y}\right) + J_1^s\ddot{\phi} \end{aligned} \tag{23d}$$

$$\begin{aligned} \delta\phi: \; & P\left(\frac{\partial u_0}{\partial x}+\frac{\partial v_0}{\partial y}\right) - P^a\left(\frac{\partial^2 w_b}{\partial x^2}+\frac{\partial^2 w_b}{\partial y^2}\right) + (T-A_{44}^s)\frac{\partial^2 w_s}{\partial x^2} + (R-A_{55}^s)\frac{\partial^2 w_s}{\partial y^2} + T^a\phi - A_{44}^s\frac{\partial^2 \phi}{\partial x^2} - A_{55}^s\frac{\partial^2 \phi}{\partial y^2} \\ & = J_1^s(\ddot{w}_b+\ddot{w}_s) + K_2^s\ddot{\phi} \end{aligned} \tag{23e}$$

2.5 Navier analytical solutions

To obtain analytical solutions, Navier's approach is used (Ebrahimi and Daman 2017). They are the partial differential equations of displacement, expressed by double Fourier series satisfying simply supported boundary conditions and written in the following form

$$u_0(x,y,t) = \sum_{m=1}^{\infty}\sum_{n=1}^{\infty} U_{mn}\cos(\lambda x)\sin(\mu y)\cdot e^{i\omega t} \tag{24a}$$

$$v_0(x,y,t) = \sum_{m=1}^{\infty}\sum_{n=1}^{\infty} V_{mn}\sin(\lambda x)\cos(\mu y)\cdot e^{i\omega t} \tag{24b}$$

$$w_b(x,y,t) = \sum_{m=1}^{\infty}\sum_{n=1}^{\infty} W_{bmn}\sin(\lambda x)\sin(\mu y)\cdot e^{i\omega t} \tag{24c}$$

$$w_s(x,y,t) = \sum_{m=1}^{\infty}\sum_{n=1}^{\infty} W_{smn}\sin(\lambda x)\sin(\mu y)\cdot e^{i\omega t} \tag{24d}$$

$$\phi(x,y,t) = \sum_{m=1}^{\infty}\sum_{n=1}^{\infty} \Phi_{mn}\, sin(\lambda x)\, sin(\mu y)\, .\, e^{i\omega t} \quad (24e)$$

where ω is the natural frequency of free vibrations of the plate, $\lambda = m\pi/a$, $\mu = n\pi/b$ and (m, n) is the frequency mode. The transverse load (q) is also represented by a double Fourier series by

$$q(x,y) = \sum_{m=1}^{\infty}\sum_{n=1}^{\infty} Q_{mn}\, sin(\lambda x)\, sin(\mu y) \quad (25a)$$

where Q_{mn} is a coefficient given below for two typical loads, such as

$$Q_{mn} = \frac{4}{ab}\int_0^a \int_0^b q(x,y)\, sin(\lambda x)\, sin(\mu y)\, dxdy = \begin{cases} q_0 \\ \dfrac{16q_0}{mn\pi^2} \end{cases} \quad (25b)$$

$$Q_{mn} = \begin{cases} q_0 \text{ for sinusoidal distributed load.} \\ \dfrac{16q_0}{mn\pi^2} \text{ for uniformly distributed load} \end{cases} \quad (25c)$$

By substituting the Eqs. (22) and (23) in (21), the equivalent system obtained is written

$$\left(\begin{bmatrix} a_{11} & a_{12} & a_{13} & a_{14} & a_{15} \\ a_{12} & a_{22} & a_{23} & a_{24} & a_{25} \\ a_{13} & a_{23} & a_{33}+\beta & a_{34}+\beta & a_{35} \\ a_{14} & a_{24} & a_{34}+\beta & a_{44}+\beta & a_{45} \\ a_{15} & a_{25} & a_{35} & a_{45} & a_{55} \end{bmatrix} - \omega^2 \begin{bmatrix} m_{11} & 0 & m_{13} & m_{14} & 0 \\ 0 & m_{22} & m_{23} & m_{24} & 0 \\ m_{13} & m_{23} & m_{33} & m_{34} & m_{35} \\ m_{14} & m_{24} & m_{34} & m_{44} & m_{45} \\ 0 & 0 & m_{35} & m_{45} & m_{55} \end{bmatrix} \right) \begin{Bmatrix} U_{mn} \\ V_{mn} \\ W_{bmn} \\ W_{smn} \\ \Phi_{mn} \end{Bmatrix} = \begin{Bmatrix} 0 \\ 0 \\ Q_{mn} \\ Q_{mn} \\ 0 \end{Bmatrix} \quad (26)$$

where

$$\begin{aligned}
&a_{11} = -(\lambda^2 A_{11} + \mu^2 A_{66}), && a_{12} = -\lambda\mu(A_{12} + A_{66}), \\
&a_{13} = \lambda^3 B_{11} + \lambda\mu^2(B_{12} + 2B_{66}), && a_{14} = \lambda^3 B_{11}^s + \lambda\mu^2(B_{12}^s + 2B_{66}^s), && a_{15} = P\lambda, \\
&a_{22} = -(\lambda^2 A_{66} + \mu^2 A_{22}), && a_{23} = \mu^3 B_{22} + \lambda^2\mu(B_{12} + 2B_{66}), \\
&a_{24} = \mu^3 B_{22}^s + \lambda^2\mu(B_{12}^s + 2B_{66}^s), && a_{25} = P\mu, \\
&a_{33} = -(\lambda^4 D_{11} + 2\lambda^2\mu^2(D_{12} + 2D_{66}) + \mu^4 D_{22}), \\
&a_{34} = -(\lambda^4 D_{11}^s + 2\lambda^2\mu^2(D_{12}^s + 2D_{66}^s) + \mu^4 D_{22}^s), \\
&a_{44} = -(\&\lambda^4 H_{11}^s + 2\lambda^2\mu^2(H_{12}^s + 2H_{66}^s) + \mu^4 H_{22}^s + \lambda^2 A_{55}^s + \mu^2 A_{44}^s), \\
&a_{55} = -(\lambda^2 A_{44}^s + \mu^2 A_{55}^s + T^a), \\
&m_{11} = m_{22} = -I_0, && m_{13} = m_{14} = \lambda I_1, \\
&m_{23} = \mu I_1, && m_{24} = \mu J_1, \\
&m_{33} = -\left(I_0 + I_2(\lambda^2 + \mu^2)\right), && m_{34} = -\left(I_0 + J_2(\lambda^2 + \mu^2)\right), \\
&m_{44} = -\left(I_0 + K_2(\lambda^2 + \mu^2)\right), && m_{35} = m_{45} = -J_1^s, && m_{55} = -K_2^s, \\
&\beta = N_{cr}(\gamma_1\lambda^2 + \gamma_2\mu^2), && N_{cr} = N_0
\end{aligned} \quad (27)$$

3. Results and discussions

The general form of the system of Eq. (26) is used to analyze the bending, free vibration and buckling, of FGMs plates with Aluminum/Alumina (Al/Al_2O_3) and Aluminum/ Zirconia (Al/ZrO_2) couples. The square and rectangular plates edges are simply supported and are subjected to a combination of a transverse mechanical load (q) and in-plane compression loads (N_0).

The results are obtained using a new function for the transverse shear deformation effect and the theoretical formulation model developed by Thai and Kim (2013) and Belabed *et al.* (2014). Several numerical examples investigating the effect of different dimensionless parameters such as the volume fraction index (p), the geometric ratios (a/h, a/b), the frequency modes (m, n) and the in-plane compression load parameters, on the deflection, the normal and tangential stresses, the natural frequency and the critical buckling load are studied. The dimensionless relationships used for P-FGMs and E-FGMs are listed below:

For P-FGMs plates

$$\bar{z}=\frac{z}{h},\qquad \bar{u}=\frac{100E_ch^3}{q_0a^4}u\left(0,\frac{b}{2},z\right),\qquad \bar{w}=\frac{10E_ch^3}{q_0a^4}w\left(\frac{a}{2},\frac{b}{2},z\right),\qquad \bar{\sigma}_x(z)=\frac{h}{q_0a}\sigma_x\left(\frac{a}{2},\frac{b}{2},z\right),$$
$$\bar{\sigma}_y(z)=\frac{h}{q_0a}\sigma_y\left(\frac{a}{2},\frac{b}{2},z\right),\qquad \bar{\tau}_{xy}(z)=\frac{h}{q_0a}\tau_{xy}(0,0,z),\qquad \bar{\beta}=\omega h\sqrt{\frac{\rho_m}{E_m}},\qquad \widehat{\omega}=\omega h\sqrt{\frac{\rho_c}{E_c}},\tag{28}$$
$$\bar{\omega}=\frac{\omega a^2}{h}\sqrt{\frac{\rho_c}{E_c}},\qquad D_0=\frac{E_ch^3}{12(1-\nu^2)},\qquad \widehat{N}_{cr}=\frac{N_{cr}b^2}{\pi^2D_0},\qquad \bar{N}_{cr}=\frac{N_{cr}a^2}{E_mh^3}$$

For E-FGMs plates

$$\bar{z}=\frac{z}{h},\qquad \bar{u}=\frac{10E_ch^3}{q_0a^4}u\left(0,\frac{b}{2},z\right),\qquad \bar{w}=\frac{10E_ch^3}{q_0a^4}w\left(\frac{a}{2},\frac{b}{2},z\right),\qquad \bar{\sigma}_x(z)=\frac{h^2}{q_0a^2}\sigma_x\left(\frac{a}{2},\frac{b}{2},z\right),$$
$$\bar{\tau}_{xy}(z)=\frac{10h^2}{q_0a^2}\tau_{xy}(0,0,z),\qquad \bar{\tau}_{xz}(z)=\frac{h}{q_0a}\tau_{xz}\left(0,\frac{b}{2},z\right),\tag{29}$$

Table 2 Comparison of the non-dimensional deflection ($\overline{w}$) of couple Aluminium/Alumina (Al/Al_2O_3) E-FGMs plates

a/h	b/a	Theories	Power-law index p					
			0.1	0.3	0.5	0.7	1	1.5
2	1	Quasi-3D (Zenkour 2007)	0.5731	0.5181	0.4679	0.4222	0.3612	0.2771
		3D (Zenkour 2007)	0.5769	0.5247	0.4766	0.4324	0.3727	0.2890
		Quasi-3D (Mantari and Soares 2012b)	0.5776	0.5222	0.4716	0.4255	0.3640	0.2792
		Present theory (Quasi-3D)	0.5780	0.5225	0.4719	0.4258	0.3642	0.2794
		Quasi-3D HSDT (Belabed *et al*. 2014)	0.5786	0.5231	0.4724	0.4262	0.3646	0.2797
		2D HSDT (Nguyen 2014)	0.6211	0.5615	0.5073	0.4579	0.3921	0.3014
		2D HSDT (Belkhodja *et al*. 2019)	0.6251	0.5645	0.5093	0.4592	0.3925	0.3008
		2D HSDT (Thai and Kim 2013)	0.6362	0.5751	0.5194	0.4687	0.4011	0.3079
		2D HSDT (Mantari and Soares 2012a)	0.6363	0.5752	0.5195	0.4687	0.4018	0.3079
		Present theory (2D)	0.6366	0.5755	0.5197	0.4690	0.4013	0.3080
	2	Quasi-3D (Zenkour 2007)	1.1880	1.0740	0.9701	0.8755	0.7494	0.5758
		3D (Zenkour,2007)	1.1944	1.0859	0.9864	0.8952	0.7727	0.6017
		Quasi-3D (Mantari and Soares 2012b)	1.1938	1.0790	0.9748	0.8797	0.7530	0.5785
		Present theory (Quasi-3D)	1.1943	1.0797	0.9752	0.8801	0.7533	0.5787
		Quasi-3D HSDT (Belabed *et al*. 2014)	1.1947	1.0801	0.9756	0.8804	0.7535	0.5789
		2D HSDT (Nguyen 2014)	1.2569	1.1367	1.0275	0.9284	0.7965	0.6153
		2D HSDT (Belkhodja *et al*. 2019)	1.2615	1.1396	1.0289	0.9285	0.7952	0.6125
		2D HSDT (Thai and Kim 2013)	1.2775	1.1553	1.0441	0.9431	0.8086	0.6238
		2D HSDT (Mantari and Soares 2012a)	1.2776	1.1553	1.0441	0.9431	0.8093	0.6238
		Present theory (2D)	1.2779	1.1556	1.0444	0.9433	0.8087	0.6238
	3	Quasi-3D (Zenkour 2007)	1.4354	1.2977	1.1722	1.0580	0.9057	0.6962
		3D (Zenkour 2007)	1.4430	1.3116	1.1913	1.0812	0.9334	0.7275
		Quasi-3D (Mantari and Soares 2012b)	1.4419	1.3035	1.1774	1.0626	0.9096	0.6991
		Present theory (Quasi-3D)	1.4424	1.3040	1.1778	1.0630	0.9099	0.6994
		Quasi-3D HSDT (Belabed *et al*. 2014)	1.4427	1.3043	1.1781	1.0633	0.9102	0.6995
		2D HSDT (Nguyen 2014)	1.5115	1.3671	1.2360	1.1169	0.9587	0.7414
		2D HSDT (Belkhodja *et al*. 2019)	1.5163	1.3699	1.2371	1.1167	0.9569	0.7380
		2D HSDT (Thai and Kim 2013)	1.5340	1.3873	1.2540	1.1329	0.9719	0.7506
		2D HSDT (Mantari and Soares 2012a)	1.5341	1.3874	1.2540	1.1329	0.9725	0.7506
		Present theory (2D)	1.5343	1.3876	1.2542	1.1331	0.9720	0.7506

Table 2 Comparison of the non-dimensional deflection ($\bar{w}$) of couple Aluminium/Alumina (Al/Al_2O_3) E-FGMs plates

a/h	b/a	Theories	Power-law index p					
			0.1	0.3	0.5	0.7	1	1.5
4	1	Quasi-3D (Zenkour 2007)	0.3475	0.3142	0.2839	0.2563	0.2196	0.1692
		3D (Zenkour 2007)	0.3490	0.3168	0.2875	0.2608	0.2253	0.1805
		Quasi-3D (Mantari and Soares 2012b)	0.3486	0.3152	0.2848	0.2571	0.2203	0.1697
		Present theory (Quasi-3D)	0.3486	0.3152	0.2848	0.2571	0.2203	0.1697
		Quasi-3D HSDT (Belabed *et al*. 2014)	0.3486	0.3152	0.2848	0.2571	0.2203	0.1697
		2D HSDT (Nguyen 2014)	0.3575	0.3235	0.2927	0.2649	0.2280	0.1775
		2D HSDT (Belkhodja *et al*. 2019)	0.3598	0.3255	0.2945	0.2664	0.2292	0.1782
		2D HSDT (Thai and Kim 2013)	0.3602	0.3259	0.2949	0.2668	0.2295	0.1785
		2D HSDT (Mantari and Soares 2012a)	0.3602	0.3259	0.2949	0.2668	0.2295	0.1785
		Present theory (2D)	0.3602	0.3259	0.2948	0.2668	0.2295	0.1785
	2	Quasi-3D (Zenkour 2007)	0.8120	0.7343	0.6635	0.5992	0.5136	0.3962
		3D (Zenkour 2007)	0.8153	0.7395	0.6708	0.6085	0.5257	0.4120
		Quasi-3D (Mantari and Soares 2012b)	0.8145	0.7365	0.6655	0.6009	0.5151	0.3973
		Present theory (Quasi-3D)	0.8145	0.7365	0.6655	0.6010	0.5151	0.3974
		Quasi-3D HSDT (Belabed *et al*. 2014)	0.8144	0.7364	0.6654	0.6009	0.5150	0.3973
		2D HSDT (Nguyen 2014)	0.8285	0.7498	0.6787	0.6145	0.5296	0.4135
		2D HSDT (Belkhodja *et al*. 2019)	0.8319	0.7528	0.6813	0.6167	0.5313	0.4146
		2D HSDT (Thai and Kim 2013)	0.8325	0.7534	0.6819	0.6173	0.5319	0.4150
		2D HSDT (Mantari and Soares 2012a)	0.8325	0.7534	0.6819	0.6173	0.5319	0.4150
		Present theory (2D)	0.8324	0.7534	0.6819	0.6173	0.5319	0.4151
	3	Quasi-3D (Zenkour 2007)	1.0094	0.9127	0.8248	0.7449	0.6385	0.4927
		3D (Zenkour 2007)	1.0134	0.9190	0.8335	0.7561	0.6533	0.5121
		Quasi-3D (Mantari and Soares 2012b)	1.0124	0.9155	0.8272	0.7470	0.6404	0.4941
		Present theory (Quasi-3D)	1.0125	0.9155	0.8273	0.7471	0.6404	0.4941
		Quasi-3D HSDT (Belabed *et al*. 2014)	1.0123	0.9154	0.8271	0.7470	0.6403	0.4941
		2D HSDT (Nguyen 2014)	1.0281	0.9305	0.8424	0.7628	0.6576	0.5137
		2D HSDT (Belkhodja *et al*. 2019)	1.0319	0.9338	0.8453	0.7653	0.6594	0.5149
		2D HSDT (Thai and Kim 2013)	1.0325	0.9345	0.8459	0.7659	0.6601	0.5154
		2D HSDT (Mantari and Soares 2012a)	1.0325	0.9345	0.8459	0.7659	0.6601	0.5154
		Present theory (2D)	1.0325	0.9345	0.8459	0.7659	0.6601	0.5154

3.1 Numerical examples - Results of the bending analysis

The stability or static deformation responses of the FGMs Al/Al_2O_3 plate subjected to bending, permit the assessment of the present theory accuracy, by neglecting the in-plane compression load (N_0 causing buckling) and the kinetic energy in the system of Eq. (26). The FGMs plate is only subjected to a transverse sinusoidal mechanical load. The dimensionless results are obtained for the in-plane axial displacement $\bar{u}$, the deflection $\bar{w}$, the normal stress $\bar{\sigma}_{xx}(z)$ and transverse shear stresses $\bar{\tau}_{xy}(z)$ and $\bar{\tau}_{xz}(z)$.

3.1.1 E-FGMs plate

Example 1. One of the major problems caused by bending is the deflection along the z axis, this is the reason why the first example is treated to verify the validity of the present theory by predicting the bending behavior of the plates of different shapes. In Table 2, the deflection results are grouped for both a square (b/a = 1) and a rectangular (b/a = 2, 3) Al/Al_2O_3, thick E-FGMs plates, tested for several material indices (p = 0, 1 to 1.5). The results obtained from the present 2D and quasi-3D models are compared with those found in literature. The present solutions are validated by comparing them to the 3D and quasi 3D HSDT (Zenkour 2007, Belabed *et al*. 2014) and the 2D-HSDT solutions (Thai and Kim 2013, Belkhodja *et al*. 2019, Nguyen 2014) shown in Table 2, and in particular with Mantari and Soares (2012b). The results of the quasi 3D HSDT and those of the present theory are found to be in good agreement. Concerning the 2D HSDT $\bar{w}$ results given by Mantari and Soares (2012a), the results of the present theory are slightly higher. This may be due to an important reason which is the presence of the transverse

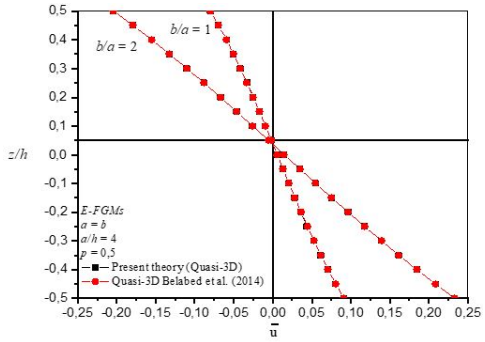

(a) In-plane axial displacement ($\bar{u}$)

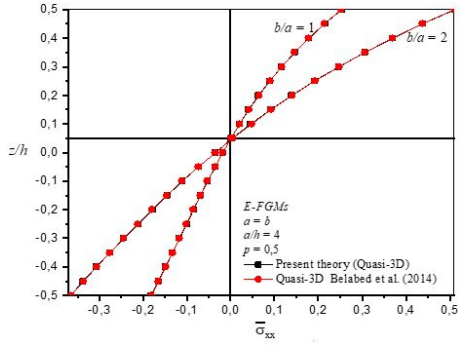

(b) In-plane stress ($\bar{\sigma}_{xx}$)

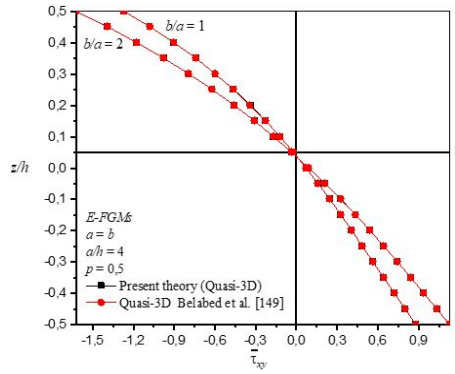

(c) In-plane shear stress ($\bar{\tau}_{xy}$)

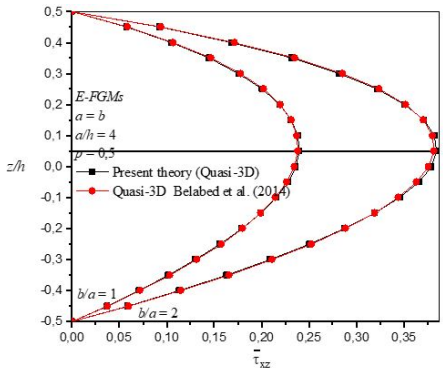

(d) In-plane stress ($\bar{\tau}_{xz}$)

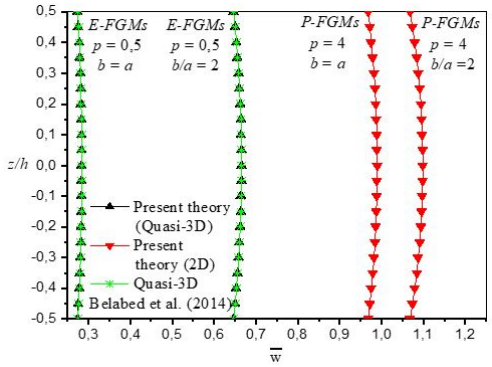

(e) Deflection ($\bar{w}$)

Fig. 3 Variation of non-dimensional displacement and stresses through the Al/Al2O3 E-FGM plates thickness

shear deformation effect in the transverse direction, materialized by the precision of the shape function, the different displacement models, the number of unknowns corresponding with or without the presence of the stretching effect. This latter along with the boundary conditions used have an important effect on the stress components in the transverse direction in the case of thick plates. The increase in the ratio (b/a) and the simultaneous decrease in the index (p) and the ratio (a/h), lead to a maximum error of the order of 0.072% in quasi-3D and 0.125% in 2D, which is negligible. In this case, the displacement $\bar{w}$ obtained becomes more significant for very thick plates (p = 1, 5, b/a = 1, a/h = 2) and (p = 1, a/h = 2). The solutions are identical for several cases when (a/h = 4).The representation of the quasi 3D HSDT results compared with those found by Belabed *et al*. (2014) in terms of the thickness variation (z/h) for two different E-FGM Al/Al_2O_3 plates, one square and another rectangular (b/a = 2), is illustrated in Figs. 3(a)-(e) for an index (p = 0.5) and width (a/h = 4). The figures show a very good agreement between the results found in all cases, confirming the accuracy of the present theory for predicting the flexural responses of E-FGM plates. It should be noted that the plane (z/h = 0.05) is an important neutral plane on which the dimensionless results of $\bar{u}$ and $\bar{\tau}_{xy}(z)$ change sign from negative values in the upper ceramic part towards positive values in the lower aluminium part. An inverse behavior is noted for the case of the normal stress $\bar{\sigma}_{xx}(z)$ in comparison with the shear stress $\bar{\tau}_{xy}(z)$. The values become more important for the rectangular E-FGMs plate on the lower tensile ductile part. The maximum shear stress $\bar{\tau}_{xz}(z)$ is obtained on the neutral plane but less important than the stresses $\bar{\tau}_{xy}(z)$ and $\bar{\sigma}_{xx}(z)$. It should be emphasized in Fig. 3(e) that, for the same plate (square or rectangle), the deflection $\bar{w}$ remains constant and

Table 3 Non-dimensional stresses and deflection of couple Aluminium/Alumina (Al/Al_2O_3) P-FGMs square plates

p	Theories	$\bar{\sigma}_{xx}$ $(h/3)$			$\bar{w}$		
		a/h = 4	a/h = 10	a/h = 100	a/h = 4	a/h = 10	a/h = 100
1	FSDT (Carrera *et al*. 2008)	0.8060	2.0150	20.1500	0.7291	0.5889	0.5625
	CPT (Carrera *et al*. 2008)	0.8060	2.0150	20.1500	0.5623	0.5623	0.5623
	Quasi-3D (Carrera *et al*. 2008)	0.6221	1.5064	14.9690	0.7171	0.5875	0.5625
	Quasi-3D (Carrera *et al*. 2011)	0.6221	1.5064	14.9690	0.7171	0.5875	0.5625
	Quasi-3D (Neves *et al*. 2012a)	0.5925	1.4945	14.9690	0.6997	0.5845	0.5624
	Quasi-3D (Neves *et al*. 2012b)	0.5910	1.4917	14.9440	0.7020	0.5868	0.5648
	Quasi-3D (Neves *et al*. 2013)	0.5911	1.4917	14.9450	0.7020	0.5868	0.5647
	Present theory (Quasi-3D)	0.5866	1.4678	14.6768	0.6917	0.5696	0.5461
	Quasi-3D HSDT (Belabed *et al*. 2014)	0.5865	1.4677	14.6762	0.6916	0.5695	0.5461
	2D HSDT (Thai and Kim 2013)	0.5812	1.4898	14.9676	0.7284	0.5890	0.5625
	Present theory (2D)	0.5813	1.4896	14.9675	0.7284	0.5889	0.5625
4	FSDT (Carrera *et al*. 2008)	0.6420	1.6049	16.0490	1.1125	0.8736	0.8286
	CPT (Carrera *et al*. 2008)	0.6420	1.6049	16.0490	0.8281	0.8281	0.8281
	Quasi-3D (Carrera *et al*. 2008)	0.4877	1.1971	11.9230	1.1585	0.8821	0.8286
	Quasi-3D (Carrera *et al*. 2011)	0.4877	1.1971	11.9230	1.1585	0.8821	0.8286
	Quasi-3D (Neves *et al*. 2012a)	0.4404	1.1783	11.9320	1.1178	0.8750	0.8286
	Quasi-3D (Neves *et al*. 2012b)	0.4340	1.1593	11.7380	1.1095	0.8698	0.8241
	Quasi-3D (Neves *et al*. 2013)	0.4330	1.1588	11.7370	1.1108	0.8700	0.8240
	Present theory (Quasi-3D)	0.4390	1.1440	11.5240	1.0985	0.8424	0.7934
	Quasi-3D HSDT (Belabed *et al*. 2014)	0.4396	1.1460	11.5443	1.0981	0.8423	0.7934
	2D HSDT (Thai and Kim 2013)	0.4449	1.1794	11.9209	1.1599	0.8815	0.8287
	Present theory (2D)	0.4449	1.1787	11.9208	1.1601	0.8818	0.8287
10	FSDT (Carrera *et al*. 2008)	0.4796	1.1990	11.9900	1.3178	0.9966	0.9360
	CPT (Carrera *et al*. 2008)	0.4796	1.1990	11.9900	0.9354	0.9354	0.9354
	Quasi-3D (Carrera *et al*. 2008)	0.3695	0.8965	8.6077	1.3745	1.0072	0.9361
	Quasi-3D (Carrera *et al*. 2011)	0.3695	0.8965	8.6077	1.3745	1.0072	0.9361
	Quasi-3D (Neves *et al*. 2012a)	0.3227	1.1783	11.9320	1.3490	0.8750	0.8286
	Quasi-3D (Neves *et al*. 2012b)	0.3108	0.8467	8.6013	1.3327	0.9886	0.9228
	Quasi-3D (Neves *et al*. 2013)	0.3097	0.8462	8.6010	1.3334	0.9888	0.9227
	Present theory (Quasi-3D)	0.3221	0.8598	8.6977	1.3357	0.9815	0.9138
	Quasi-3D HSDT (Belabed *et al*. 2014)	0.3231	0.8622	8.7215	1.3353	0.9812	0.9135
	2D HSDT (Thai and Kim 2013)	0.3259	0.8785	8.9060	1.3909	1.0087	0.9362
	Present theory (2D)	0.3258	0.8779	8.9058	1.3909	1.0089	0.9362

almost stable, except that the rectangular plate results in important values twice as large as a square plate.

3.1.2 P-FGMs plate

Example 2. In order to predict the validity of this HSDT theory in 2D and quasi 3D, the dimensionless results of the bending responses in terms of the deflection $\bar{w}$ and the normal stress $\bar{\sigma}_{xx}(h/3)$ were compared with different theories as shown in Table 3. In this case, the square Al/Al_2O_3 P-FGMs plate subjected to bending, with different material indices of the moderately rigid material (p = 1, 4, 10), for different thicknesses z of the thick plate (a/h = 4), moderately thick (a/h = 10) and thin (a/h = 100) respectively. The obtained dimensionless results are compared with solutions given by different theories such as CPT and FSDT (Carrera *et al*. 2008), the quasi-3D theories taking into account the effect of transverse shear and normal deformation (Neves *et al*. 2012a, b, 2013, Belabed *et al*. 2014), as well as those predicted by 2D-HSDT of Thai and Kim (2013). It should be noted that the results of the quasi-3D and 2D theories obtained have shown good prediction and good agreement, respectively with different solutions of the theories presented in Table 3, in particular Belabed *et al*. (2014) and Thai and Kim (2013). The maximum error rate produced is of the order of 0.036%, 0.034% and 0.031%, 0.068%, respectively for (p = 4, a/h =

4 and 10) and (p = 10, a/h = 4, 10). It should be noted that when the power index (p) increases widely and (a/h) decreases, the plate becomes less rigid and thicker, the deflection $\bar{w}$ increases and the normal stress $\bar{\sigma}_{xx}(z)$ decreases. The calculated error rate tends to increase and becomes more important for the less rigid plates to the more ductile and thicker ones. From Table 3, it should be noted that the more the plate is ductile the more it is deformable, as well as the greater the thickness, the more the effects of shear deformation are proportional. The relative error of the deflection $\bar{w}$ is almost zero between the current values of Quasi-3D HSDT, CPT and FSDT given by Carrera *et al*. (2008, 2011). It is respectively of the order of 0,036% and 0%, which is negligible for the more rigid and thin plates (p = 1, a/h = 100).

Example 3. A moderately thick, rigid and moderately rigid square Al/Al_2O_3 P-FGMs plate (p = 1, 2, 4, 8) is considered. More details and explanations are reported in this 2D HSDT theory, including the results of displacements

Table 4 Non-dimensional deflections and stresses of couple Aluminium/Alumina (Al/Al_2O_3) P-FGMs square plates (a/h = 10)

p	Theories	$\bar{u}(-h/4)$	$\bar{w}$	$\bar{\sigma}_{xx}(h/3)$	$\bar{\tau}_{xy}(-h/3)$	$\bar{\tau}_{xz}(h/6)$
1	2D SSDT (Zenkour 2006)	0.6626	0.5889	1.4894	0.6110	0.2622
	Quasi-3D (Carrera *et al*. 2011)	0.6436	0.5875	1.5062	0.6081	0.2510
	Quasi-3D (Wu *et al*. 2011)	0.6436	0.5876	1.5061	0.6112	0.2511
	2D TSDT (Wu and Li 2010)	0.6414	0.5890	1.4898	0.6111	0.2599
	2D HSDT (Thai and Kim 2013)	0.6414	0.5890	1.4898	0.6111	0.2608
	Present theory (2D)	0.6411	0.5889	1.4896	0.6111	0.2615
	2D (Belkhodja *et al*. 2019)	0.6410	0.5889	1.4893	0.6111	0.2631
	2D HSDT (Nguyen 2014)	0.6401	0.5883	1.4892	0.6110	0.2552
	2D HSDT (Mantari *et al*. 2012)	0.6398	0.5880	1.4888	0.6109	0.2566
4	2D SSDT (Zenkour 2006)	0.9281	0.7573	1.3954	0.5441	0.2763
	Quasi-3D (Carrera *et al*. 2011)	0.9012	0.7570	1.4147	0.5421	0.2496
	Quasi-3D (Wu *et al*. 2011)	0.9013	0.7571	1.4133	0.5436	0.2495
	2D TSDT (Wu and Li 2010)	0.8984	0.7573	1.3960	0.5442	0.2721
	2D HSDT (Thai and Kim 2013)	0.8984	0.7573	1.3960	0.5442	0.2737
	Present theory (2D)	0.8979	0.7573	1.3957	0.5441	0.2753
	2D (Belkhodja *et al*. 2019)	0.8978	0.7573	1.3954	0.5442	0.2770
	2D HSDT (Nguyen 2014)	0.8961	0.7567	1.3947	0.5439	0.2721
	2D HSDT (Mantari *et al*. 2012)	0.8957	0.7564	1.3940	0.5438	0.2741
10	2D SSDT (Zenkour 2006)	1.0941	0.8819	1.1783	0.5667	0.2580
	Quasi-3D (Carrera *et al*. 2011)	1.0541	0.8823	1.1985	0.5666	0.2362
	Quasi-3D (Wu *et al*. 2011)	1.0541	0.8823	1.1841	0.5671	0.2362
	2D TSDT (Wu and Li 2010)	1.0502	0.8815	1.1794	0.5669	0.2519
	2D HSDT (Thai and Kim 2013)	1.0502	0.8815	1.1794	0.5669	0.2537
	Present theory (2D)	1.0495	0.8818	1.1787	0.5668	0.2566
	2D (Belkhodja *et al*. 2019)	1.0493	0.8818	1.1783	0.5668	0.2586
	2D HSDT (Nguyen 2014)	1.0466	0.8818	1.1766	0.5664	0.2593
	2D HSDT (Mantari *et al*. 2012)	1.0457	0.8814	1.1755	0.5662	0.2623
8	2D SSDT (Zenkour 2006)	1.1340	0.9750	0.9466	0.5856	0.2121
	Quasi-3D (Carrera *et al*. 2011)	1.0830	0.9738	0.9687	0.5879	0.2262
	Quasi-3D (Wu *et al*. 2011)	1.0830	0.9739	0.9622	0.5883	0.2261
	2D TSDT (Wu and Li 2010)	1.0763	0.9747	0.9477	0.5858	0.2087
	2D HSDT (Thai and Kim 2013)	1.0763	0.9746	0.9477	0.5858	0.2088
	Present theory (2D)	1.0755	0.9749	0.9470	0.5857	0.2109
	2D (Belkhodja *et al*. 2019)	1.0752	0.9750	0.9466	0.5857	0.2129
	2D HSDT (Nguyen 2014)	1.0719	0.9744	0.9444	0.5852	0.2117
	2D HSDT (Mantari *et al*. 2012)	1.0709	0.9737	0.9431	0.5850	0.2140

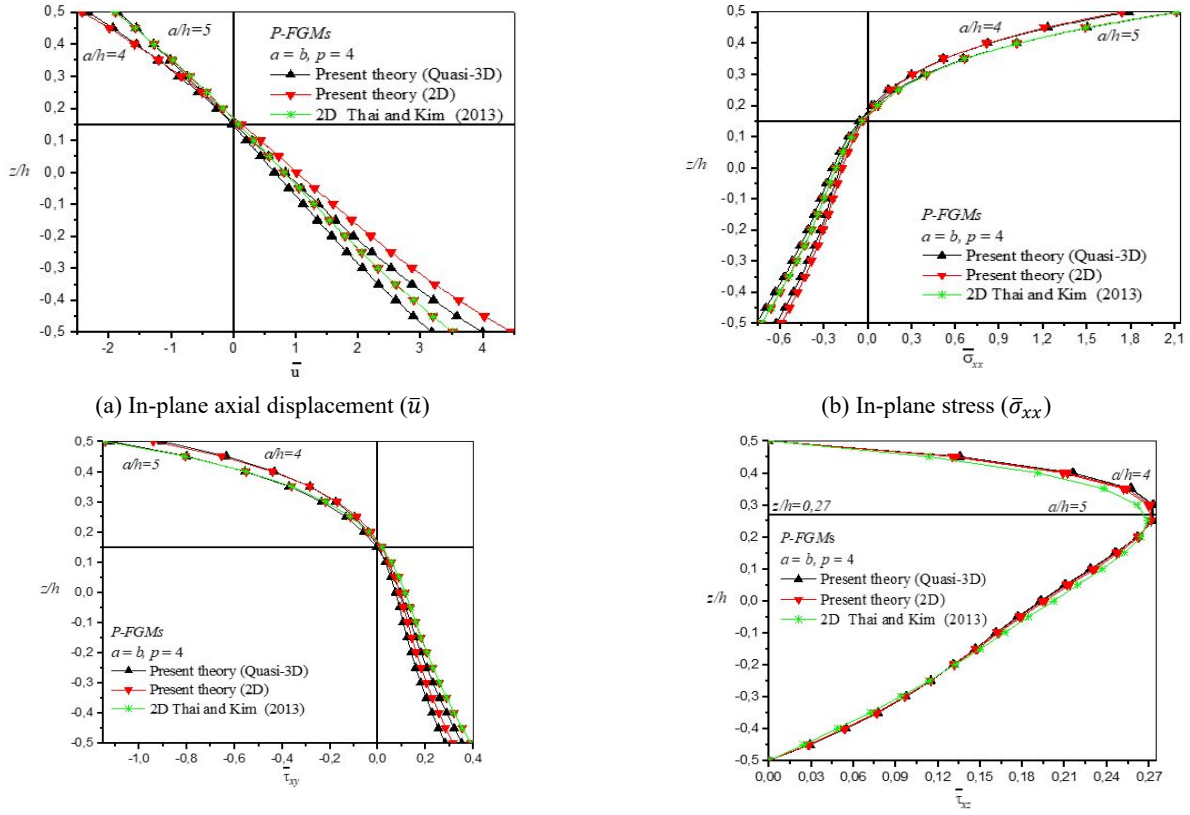

(a) In-plane axial displacement ($\bar{u}$)

(b) In-plane stress ($\bar{\sigma}_{xx}$)

(c) In-plane shear stress ($\bar{\tau}_{xy}$)

(d) In-plane stress ($\bar{\tau}_{xz}$)

Fig. 4 Variation of non-dimensional displacement and stresses through the Al/Al_2O_3 plates thickness

and dimensionless stresses of $\bar{u}$, $\bar{w}$, $\bar{\sigma}_{xx}(z)$, $\bar{\tau}_{xz}(z)$ and $\bar{\tau}_{xy}(z)$ are grouped in Table 4. The moderately thick and square Al/Al_2O_3 P-FGMs plates showed very good agreement with various results of quasi-3D (Carrera *et al.* 2011, Wu *et al.* 2011), as well as 2D theories (Zenkour 2006, Thai and Kim 2013, Wu and Li 2010, Mantari *et al.* 2012, Nguyen 2014), in particular Belkhodja *et al.* (2019), where the maximum error rate is of the order of 0.028%, 0.010%, 0.042%, 0.939 and 0.018%, which is negligible for the power indices $(p = 8)$ and $(p = 4)$, respectively. The increase in the power index (p) leads to the increase in dimensionless displacements $\bar{u}(-h/4)$ and $\bar{w}$ and therefore to the reduction of the normal stress $\bar{\sigma}_{xx}(h/3)$. The shear stresses $\bar{\tau}_{xy}(z)$ and $\bar{\tau}_{xz}(z)$ exhibit a minimum and maximum peak value respectively at the index $(p = 2)$, and the error rate is found independent of the stress values obtained by different theories. The displacement $\bar{u}$, the normal stress $\bar{\sigma}_{xx}(z)$ and the shear stresses $\bar{\tau}_{xy}(z)$ and $\bar{\tau}_{xz}(z)$ as a function of the change in thickness (z/h) for a rigid thick square P-FGMs plate $(p = 4,\ a/h = 4,\ 5)$ are illustrated in Figs. 4(a)-(c). It should be noted that a good correlation is presented with the results found from 2D HSDT of Thai and Kim (2013) for the entire thickness of the plate, confirming the accuracy of the present theory making it possible to predict good bending responses of the FGM plates. The trends of the quasi-3D results for the thick plate (a/h = 4 and 5), present a good agreement with the trends of the 2D results only for the more rigid upper part of the plate P-FGM $(z/h > 0.15)$. It could be observed that $\bar{u}$ and $\bar{\tau}_{xy}(z)$ become more significant for the more ductile lower part of the P-FGMs $(z/h < 0.15)$ plate. Below this axis, $\bar{u}$ and $\bar{\tau}_{xy}(z)$ have positive values and vice versa for the case of the stress $\bar{\sigma}_{xx}(z)$. It is clear that the lower part is more deformable (flexible) than the upper part made of ceramic. In this case, bending leads to two important phenomena; compression leads to negative values and stretching to positive values. The trends shown in Fig. 4(d), indicate that the results obtained from the transverse shear stress $\bar{\tau}_{xz}(z)$ through the well correlated theories quasi-3D and 2D HSDT, slightly in default on the neutral plane (z/h = 0.25, where the maximum peak is located). The maximum value of $\bar{\tau}_{xz}(z)$ is less important than $\bar{\sigma}_{xx}(z)$ and $\bar{\tau}_{xy}(z)$. Figs. 5(a) and (b) show the comparison of the evolution of the deflection $\bar{w}$ as a function of the power index and the geometric ratio (a/h), of a thick square P-FGM plate for different theories quasi-3D, 2D HSDT of Belabed *et al.* (2014) and Thai and Vo (2013). It should be noted that the displacement $\bar{w}$ becomes more important with the increase in the power index and decrease in the geometric ratio (a/h). The maximum deflection $\bar{w}$ is obtained for more ductile P-FGM thick plates $(a/h = 5)$. The increase of the $\bar{w}$ curve is more important when the power index $(p < 2)$. The displacement $\bar{w}$ tends to become asymptotic as the plate becomes more ductile. On Fig. 5(b), for the P-FGM plate, the increasing in the power index and reduction in the geometric ratio (a/h) lead to the increase of $\bar{w}$ in the interval $(a/h \in]2,\ 10[)$.

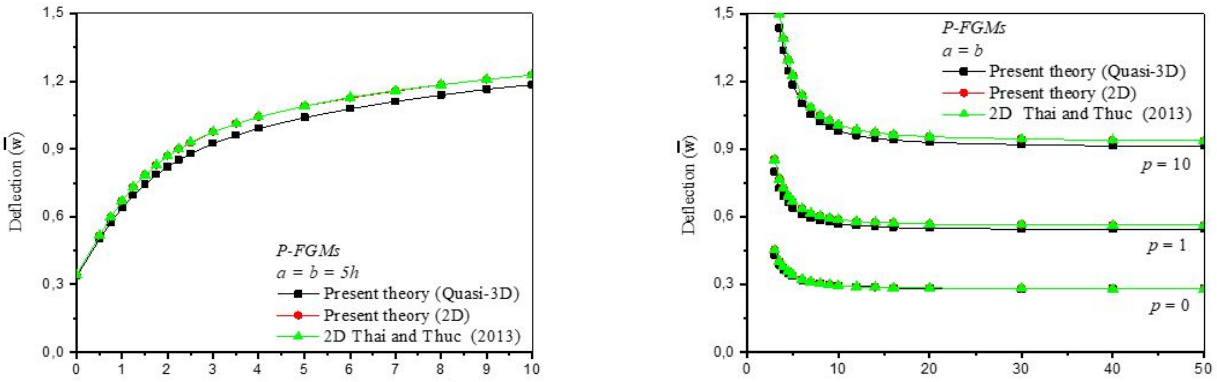

(a) p (b) a/h

Fig. 5 Comparison of variation of non-dimensional deflection $\bar{w}$ of Al/Al_2O_3 P-FGM plate versus: (a) power law index (p); and (b) side-to-thickness ratio (a/h)

Table 5 Non-dimensional fundamental frequency ($\bar{\beta}$) of couple Aluminium/Zirconia (Al/ZrO_2) MT-FGMs square plates, for ceramic plate $\bar{\beta} = \omega h\sqrt{\rho_c/E}_c$

Theories	Ceramic		$p = 1$			$a/h = 5$		
	$a/h = \sqrt{10}$	$a/h = 10$	$a/h = 5$	$a/h = 10$	$a/h = 20$	$p = 2$	$p = 3$	$p = 5$
2D HSDT (Thai and Kim 2013)	0.4623	0.0577	0.2169	0.0592	0.0152	0.2178	0.2193	0.2206
3D (Vel and Batra 2004)	0.4658	0.0578	0.2192	0.0596	0.0153	0.2197	0.2211	0.2225
Quasi-3D (Belabed *et al*. 2014)	0.4659	0.0578	0.2192	0.0597	0.0153	0.2201	0.2214	0.2225
Present theory (Quasi-3D)	0.4660	0.0578	0.2193	0.0597	0.0153	0.2201	0.2214	0.2225
Quasi-3D (Neves *et al*. 2012a)	-	-	0.2193	0.0596	0.0153	0.2198	0.2212	0.2225
Quasi-3D (Neves *et al*. 2012b)	-	-	0.2193	0.0596	0.0153	0.2201	0.2216	0.2230
Quasi-3D (Neves *et al*. 2013)	-	-	0.2193	-	-	0.2200	0.2215	0.2230

3.2 Numerical examples and results of free vibration analysis

This part is devoted to the analysis of the plate in free vibrations, in order to test the accuracy of the present theory for both the P-FGMs aluminum/zirconia (Al/ZrO_2) and aluminum/alumina (Al/Al_2O_3) plates. Thus, the vibration problem is treated by neglecting the transverse sinusoidal mechanical load (q) and the compression in-planeload (N_0) of Eq. (17).

Example 4. The dimensionless results of natural frequencies ($\bar{\beta}$) obtained are presented in Table 5, for different aluminum/zirconia (Al/ZrO_2) MT-FGM plates of homogeneous pure ceramic and several power indices (p = 0 à 5). Different thicknesses of the square plate are considered: thick plates ($a/h = \sqrt{10}$, 5), moderately thick (a/h = 10) and thin (a/h = 20). The results generated from the present theory quasi-3D are compared with those of quasi-3D HSDT of Belabed *et al*. (2014); Neves *et al*. (2012a, b, 2013) and Vel and Batra (2004) and 2D HSDT of Thai and Kim (2013). It should be noted that the results obtained are in very good agreement with the solutions of the theories mentioned in the bibliographic references, in particular with the quasi-3D HSDT theory of Belabed *et al*. (2014) even for thick and less rigid MT-FGM plates, where $\bar{\beta}$ becomes more important. The maximum error rate between the solutions of the present model and of Belabed *et al*. (2014) is around 0.0456% for (a/h = 5, p = 1), which is negligible.

Example 5. The fundamental frequencies $\hat{\omega}$ of free vibrations are calculated in Table 6, for different Al/Al_2O_3 P-FGM homogeneous ceramic plates starting from the most to the least rigid according to the power index (p = 0.5, 1, 4, 10). Different thicknesses of the square plate are considered: thick, moderately thick and thin (a/h = 2, 5, 10, 20) for the first three vibratory modes ((m, n) = 1 (1, 1), 2 (1,2), 3 (2, 2)) in 2D and Quasi-3D. The results are compared with the FSDT (Hosseini-Hashemi *et al*. 2011b), quasi-3D HSDT (Belabed *et al*. 2014, Matsunaga 2008) and 2D HSDT theories (Thai and Kim 2013, Nguyen 2014, Hosseini-Hashemi *et al*. 2011a, Belkhodja *et al*. 2019). It is clear that the results obtained for thin plates are identical to those of 2D HSDT theory and very close in comparison with quasi-3D HSDT solutions. For this type of plate the effect of the transverse shear deformation is not significant and the various theories present more precision and convergence. The results obtained for the thick plate within the quasi-3D and 2D HSDT theories are in good agreement with the solutions of Belabed *et al*. (2014) and Thai and Kim (2013). The maximum error rate is not significant and is approximately 1,943% (p = 0.5, a/h = 2, mode 2), and 0.668% (p = 0, a/h = 5, mode 3), respectively. It should be

noted that the values of $\hat{\omega}$ increase with decreasing values of the power index (p) and geometric ratio (a/h), as well as the increase in the frequency modes.

Example 6. In order to verify the accuracy of the present theory, the results in Table 7 obtained from the dimensionless fundamental frequencies of the free vibrations $\bar{\omega}$ of a rectangular Al/Al_2O_3, P-FGMs plates of homogeneous pure ceramic of different power indices (more to less rigid p = 0 à 10) and for different thicknesses (a/h = 5, 10, 20) are compared. The first four frequency modes are considered (m, n) = 1 (1, 1), 2 (1, 2), 3 (1, 3), 4 (2, 1).

It should be noted that in comparison with the theories

Table 6 Comparison of the first three non-dimensional fundamental frequencies ($\hat{\omega}$) of couple Aluminium/Alumina (Al/Al_2O_3) P-FGMs square plates

a/h	Mode (m,n)	Theories	Power-law index p				
			Ceramic	0.5	1	4	10
2	1(1,1)	Quasi-3D HSDT (Belabed *et al*. 2014)	0.9414	0.8248	0.7516	0.6056	0.5495
		Present theory (Quasi-3D)	0.9411	0.8247	0.7514	0.6055	0.5494
		Quasi-3D (Matsunaga 2008)	0.9400	0.8233	0.7477	0.5997	0.5460
		2D HSDT (Thai and Kim 2013)	0.9297	0.8110	0.7356	0.5924	0.5412
		Present theory (2D)	0.9295	0.8109	0.7355	0.5926	0.5412
	2(1,2)	Quasi-3D HSDT (Belabed *et al*. 2014)	1.7512	1.5798	1.4164	1.1147	0.9958
		Present theory (Quasi-3D)	1.7503	1.5491	1.4156	1.1143	0.9954
		Quasi-3D (Matsunaga 2008)	1.7406	1.5425	1.4078	1.1040	0.9847
		2D HSDT (Thai and Kim 2013)	1.7233	1.5192	1.3844	1.0919	0.9807
		Present theory (2D)	1.7219	1.5183	1.3834	1.0918	0.9802
5	1(1,1)	Present theory (Quasi-3D)	0.2122	0.1826	0.1660	0.1409	0.1318
		Quasi-3D HSDT (Belabed *et al*. 2014)	0.2121	0.1819	0.1640	0.1383	0.1306
		Quasi-3D (Matsunaga 2008)	0.2121	0.1819	0.1640	0.1383	0.1306
		2D HSDT (Nguyen 2014)	0.2117	0.1807	0.1634	0.1378	0.1303
		2D (Belkhodja *et al*. 2019)	0.2113	0.1808	0.1632	0.1378	0.1300
		TSDT (Hosseini-Hashemi *et al*. 2011a)	0.2113	0.1807	0.1631	0.1378	0.1301
		2D HSDT (Thai and Kim 2013)	0.2113	0.1807	0.1631	0.1378	0.1301
		Present theory (2D)	0.2113	0.1807	0.1631	0.1378	0.1300
		FSDT (Hosseini-Hashemi *et al*. 2011b)	0.2112	0.1805	0.1631	0.1397	0.1324
	2(1,2)	Present theory (Quasi-3D)	0.4663	0.4044	0.3679	0.3048	0.2812
		Quasi-3D HSDT (Belabed *et al*. 2014)	0.4659	0.4041	0.3676	0.3047	0.2811
		Quasi-3D (Matsunaga 2008)	0.4658	0.4040	0.3644	0.3000	0.2790
		2D HSDT (Nguyen 2014)	0.4645	0.4004	0.3622	0.2981	0.2783
		2D (Belkhodja *et al*. 2019)	0.4625	0.3990	0.3609	0.2980	0.2769
		TSDT (Hosseini-Hashemi *et al*. 2011a)	0.4623	0.3989	0.3607	0.2980	0.2771
		2D HSDT (Thai and Kim 2013)	0.4623	0.3989	0.3607	0.2980	0.2771
		Present theory (2D)	0.4623	0.3989	0.3607	0.2979	0.2771
		FSDT (Hosseini-Hashemi *et al*. 2011b)	0.4618	0.3978	0.3604	0.3049	0.2856
	3(2,2)	Present theory (Quasi-3D)	0.6764	0.5896	0.5368	0.4382	0.4010
		Quasi-3D HSDT (Belabed *et al*. 2014)	0.6757	0.5890	0.5362	0.4381	0.4008
		Quasi-3D (Matsunaga 2008)	0.6688	0.5803	0.5254	0.4284	0.3948
		2D HSDT (Nguyen 2014)	0.6734	0.5836	0.5286	0.4291	0.3974
		2D (Belkhodja *et al*. 2019)	0.6694	0.5806	0.5258	0.4285	0.3946
		TSDT (Hosseini-Hashemi *et al*. 2011a)	0.6676	0.5779	0.5245	0.4405	0.4097
		2D HSDT (Thai and Kim 2013)	0.6734	0.5836	0.5286	0.4291	0.3974
		Present theory (2D)	0.6689	0.5803	0.5255	0.4282	0.3948
		FSDT (Hosseini-Hashemi *et al*. 2011b)	0.6688	0.5803	0.5254	0.4284	0.3948

Table 6 Continued

a/h	Mode (m,n)	Theories	Power-law index p				
			Ceramic	0.5	1	4	10
10	1(1,1)	Present theory (Quasi-3D)	0.0578	0.0494	0.0449	0.0389	0.0368
		Quasi-3D HSDT (Belabed *et al*. 2014)	0.0578	0.0494	0.0449	0.0389	0.0368
		Quasi-3D (Matsunaga 2008)	0.0578	0.0492	0.0443	0.0381	0.0364
		2D HSDT (Nguyen 2014)	0.0577	0.0490	0.0442	0.0381	0.0364
		2D (Belkhodja *et al*. 2019)	0.0577	0.0490	0.0442	0.0381	0.0364
		TSDT (Hosseini-Hashemi *et al*. 2011a)	0.0577	0.0490	0.0442	0.0381	0.0364
		2D HSDT (Thai and Kim 2013)	0.0577	0.0490	0.442	0.0381	0.0364
		Present theory (2D)	0.0577	0.0490	0.0442	0.0381	0.0364
		FSDT (Hosseini-Hashemi *et al*. 2011b)	0.0577	0.0490	0.0442	0.0382	0.0366
	2(1,2)	Present theory (Quasi-3D)	0.1382	0.1185	0.1078	0.0923	0.0868
		Quasi-3D HSDT (Belabed *et al*. 2014)	0.1381	0.1184	0.1077	0.0923	0.0868
		Quasi-3D (Matsunaga 2008)	0.1381	0.1180	0.1063	0.0905	0.0859
		2D HSDT (Nguyen 2014)	0.1379	0.1175	0.1060	0.0902	0.0857
		2D (Belkhodja *et al*. 2019)	0.1377	0.1174	0.1059	0.0902	0.0856
		TSDT (Hosseini-Hashemi *et al*. 2011a)	0.1377	0.1174	0.1059	0.0903	0.0856
		2D HSDT (Thai and Kim 2013)	0.1377	0.1174	0.1059	0.0903	0.0856
		Present theory (2D)	0.1377	0.1174	0.1059	0.0902	0.0856
		FSDT (Hosseini-Hashemi *et al*. 2011b)	0.1376	0.1173	0.1059	0.0911	0.0867
	3(2,2)	Present theory (Quasi-3D)	0.2124	0.1827	0.1661	0.1410	0.1319
		Quasi-3D HSDT (Belabed *et al.* 2014)	0.2121	0.1825	0.1659	0.1409	0.1318
		Quasi-3D (Matsunaga 2008)	0.2117	0.1810	0.1634	0.1378	0.1303
		2D (Belkhodja *et al*. 2019)	0.2113	0.1807	0.1632	0.1378	0.1300
		2D HSDT (Nguyen 2014)	0.2113	0.1807	0.1631	0.1378	0.1301
		2D HSDT (Thai and Kim 2013)	0.2113	0.1807	0.1631	0.1378	0.1301
		Present theory (2D)	0.2113	0.1807	0.1631	0.1378	0.1300
20	1(1,1)	Present theory (Quasi-3D)	0.0148	0.0127	0.0115	0.0100	0.0095
		Quasi-3D HSDT (Belabed *et al*. 2014)	0.0148	0.0126	0.0115	0.0100	0.0095
		Quasi-3D (Matsunaga 2008)	0.0148	0.0125	0.0113	0.0098	0.0094
		2D (Belkhodja *et al*. 2019)	0.0148	0.0125	0.0113	0.0098	0.0094
		2D HSDT (Nguyen 2014)	0.0148	0.0125	0.0113	0.0098	0.0094
		2D HSDT (Thai and Kim 2013)	0.0148	0.0125	0.0113	0.0098	0.0094
		Present theory (2D)	0.0148	0.0125	0.0113	0.0098	0.0094
		FSDT (Hosseini *et al*. 2011b)	0.0148	0.0125	0.0113	0.0098	0.0094
	2(1,2)	Present theory (Quasi-3D)	0.0366	0.0313	0.0284	0.0247	0.0234
		2D (Belkhodja *et al*. 2019)	0.0365	0.0310	0.0279	0.0241	0.0231
		2D HSDT (Nguyen 2014)	0.0365	0.0310	0.0279	0.0241	0.0231
		Present theory (2D)	0.0365	0.0310	0.0279	0.0241	0.0231
	3(2,2)	Present theory (Quasi-3D)	0.0579	0.0495	0.0450	0.0390	0.0369
		2D (Belkhodja *et al*. 2019)	0.0577	0.0490	0.0442	0.0381	0.0364
		2D HSDT (Nguyen 2014)	0.0577	0.0490	0.0442	0.0381	0.0364
		Present theory (2D)	0.0577	0.0490	0.0442	0.0381	0.0364

FSDT (Hosseini-Hashemi *et al*. 2011b) and 2D HSDT (Hosseini-Hashemi *et al*. 2011a, Thai and Vo 2013, Nguyen 2014, Belkhodja *et al*. 2019) a very good agreement between the results and the maximum error rate is around 0.069% compared to the values obtained by Thai and Vo (2013) for (p = 5, a/h = 5, mode 4). In the case of thin plates, the error

Table 7 Comparison of the first four non-dimensional frequencies ($\bar{\omega}$) of rectangular couple Aluminium/Alumina (Al/Al_2O_3) P-FGMs plate ($b = 2a$)

a/h	Mode (m,n)	Theories	Power-law index p				
			Ceramic	0.5	1	5	10
10	1(1,1)	2D HSDT (Nguyen 2014)	3.4464	2.9380	2.6509	2.2260	2.1432
		2D (Belkhodja *et al*. 2019)	3.4417	2.9350	2.6480	2.2269	2.1401
		2D TSDT (Hosseini-Hashemi *et al*. 2011a)	3.4412	2.9347	2.6475	2.2272	2.1407
		2D HSDT (Thai and Vo 2013)	3.4416	2.9350	2.6478	2.2260	2.1403
		Present theory (2D)	3.4413	2.9347	2.6476	2.2268	2.1406
		FSDT (Hosseini-Hashemi *et al*. 2011b)	3.4409	2.9322	2.6473	2.2528	2.1677
	2(1,2)	2D HSDT (Nguyen 2014)	5.2932	4.5258	4.0860	3.3919	3.2574
		2D (Belkhodja *et al*. 2019)	5.2824	4.5188	4.0792	3.3932	3.2501
		2D TSDT (Hosseini-Hashemi *et al*. 2011a)	5.2813	4.5180	4.0781	3.3938	3.2514
		2D HSDT (Thai and Vo 2013)	5.2822	4.5187	4.0787	3.3914	3.2506
		Present theory (2D)	5.2814	4.5181	4.0782	3.3931	3.2511
		FSDT (Hosseini-Hashemi *et al*. 2011b)	5.2802	4.5122	4.0773	3.4492	3.3094
	3(1,3)	2D TSDT (Hosseini-Hashemi *et al*. 2011a)	8.0749	6.9366	6.2663	5.1425	4.9055
		2D HSDT (Thai and Vo 2013)	8.0772	6.9384	6.2678	5.1378	4.9044
		Present theory (2D)	8.0752	6.9369	6.2665	5.1411	4.9051
		FSDT (Hosseini-Hashemi *et al*. 2011b)	8.0710	6.9231	6.2636	5.2579	5.0253
	4(2,1)	2D TSDT (Hosseini-Hashemi *et al*. 2011a)	10.1164	8.7138	7.8762	6.4074	6.0954
		2D HSDT (Thai and Vo 2013)	10.1201	8.7167	7.8787	6.4010	6.0942
		Present theory (2D)	10.1169	8.7143	7.8766	6.4054	6.0949
		FSDT (Hosseini-Hashemi *et al*. 2011b)	9.7416	8.6926	7.8711	6.5749	5.7518
	1(1,1)	2D HSDT (Nguyen 2014)	3.6533	3.0996	2.7946	2.3911	2.3118
		2D (Belkhodja *et al*. 2019)	3.6518	3.0991	2.7938	2.3913	2.3108
		2D TSDT (Hosseini-Hashemi *et al*. 2011a)	3.6518	3.0990	2.7937	2.3916	2.3110
		2D HSDT (Thai and Vo 2013)	3.6519	3.0991	2.7937	2.3912	2.3108
		Present theory (2D)	3.6518	3.0991	2.7937	2.3913	2.3109
		FSDT (Hosseini-Hashemi *et al*. 2011b)	3.6518	3.0983	2.7937	2.3998	2.3197
20	2(1,2)	2D HSDT (Nguyen 2014)	5.7731	4.9031	4.4216	3.7671	3.6388
		2D (Belkhodja *et al*. 2019)	5.7697	4.9016	4.4194	3.7674	3.6364
		2D TSDT (Hosseini-Hashemi *et al*. 2011a)	5.7694	4.9014	4.4192	3.7682	3.6368
		2D HSDT (Thai and Vo 2013)	5.7697	4.9016	4.4194	3.7673	3.6365
		Present theory (2D)	5.7696	4.9016	4.4193	3.7675	3.6365
		FSDT (Hosseini-Hashemi *et al*. 2011b)	5.7693	4.8997	4.4192	3.7881	3.6580
	3(1,3)	2D TSDT (Hosseini-Hashemi *et al*. 2011a)	9.1880	7.8189	7.0515	5.9765	5.7575
		2D HSDT (Thai and Vo 2013)	9.1887	7.8194	7.0519	5.9742	5.7566
		Present theory (2D)	9.1884	7.8192	7.0517	5.9747	5.7568
		FSDT (Hosseini *et al*., 2011b)	9.1876	7.8145	7.0512	6.0247	5.8086
	4(2,1)	2D TSDT (Hosseini-Hashemi *et al*. 2011a)	11.8315	10.0810	9.0933	7.6731	7.3821
		2D HSDT (Thai and Vo 2013)	11.8326	10.0818	9.0940	7.6696	7.3808
		Present theory (2D)	11.8321	10.0815	9.0937	7.6704	7.3811
		FSDT (Hosseini-Hashemi *et al*. 2011b)	11.8310	10.0740	9.0928	7.7505	7.4639

is almost zero since the shear deformation is negligible. It should be noted that the dimensionless frequency $\bar{\omega}$ increases when the material becomes less and less ductile, in other words when the power index (p) decreases. Furthermore, the increase in the ratio (a/h) and frequency modes, leading therefore to an increase in the plate natural

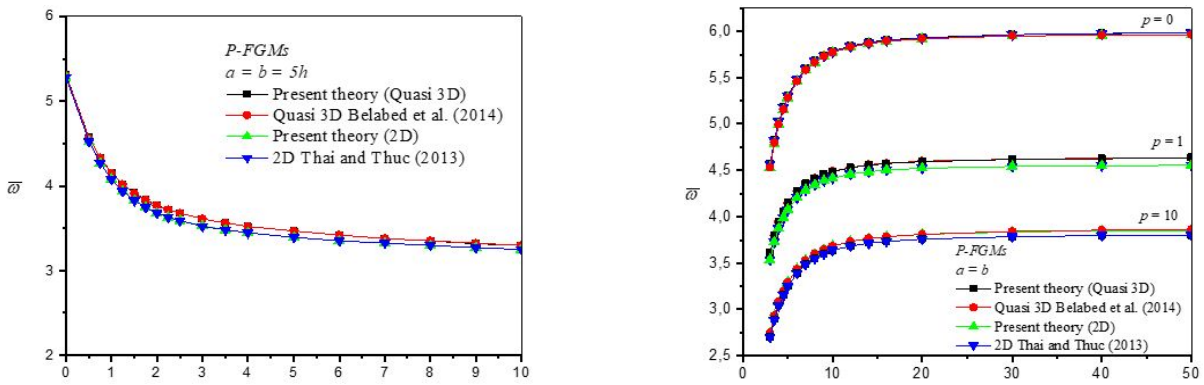

(a) p (b) a/h

Fig. 6 Variation of non-dimensional fundamental frequency ($\bar{\omega}$) of Al/Al_2O_3 plates versus: (a) power law index (p); and (b) side-to-thickness ratio (a/h)

Table 8 Comparison of non-dimensional critical buckling load ($\widehat{N}_{cr}$) of isotropic couple Aluminium/Alumina (Al/Al_2O_3) P-FGMs plate under different loading types (p = 0)

a /b	h/b	Theories	Loading mode ($\gamma1, \gamma2$)		
			1(-1,0)	2(0,-1)	3(-1,-1)
1	0.1	FSDT (Shufrin and Eisenberger 2005)	3.7865	3.7865	1.8932
		2D TSDT (Shufrin and Eisenberger 2005)	3.7866	3.7866	1.8933
		Present theory (2D)	3.7868	3.7868	1.8934
		2D HSDT (Thai and Vo 2013)	3.7869	3.7869	1.8935
		Present theory (Quasi-3D)	3.8488	3.8488	1.9244
	0.2	FSDT (Shufrin and Eisenberger 2005)	3.2637	3.2637	1.6319
		2D TSDT (Shufrin and Eisenberger 2005)	3.2653	3.2653	1.6327
		Present theory (2D)	3.2655	3.2655	1.6327
		2D HSDT (Thai and Vo 2013)	3.2666	3.2666	1.6333
		Present theory (Quasi-3D)	3.4368	3.4368	1.7184
	0.3	FSDT (Shufrin and Eisenberger 2005)	2.6533	2.6533	1.3266
		2D TSDT (Shufrin and Eisenberger 2005)	2.6586	2.6586	1.3293
		Present theory (2D)	2.6586	2.6586	1.3293
		2D HSDT (Thai and Vo 2013)	2.6612	2.6612	1.3306
		Present theory (Quasi-3D)	2.8890	2.8890	1.4445
	0.4	FSDT (Shufrin and Eisenberger 2005)	1.9196	1.9196	1.0513
		2D TSDT (Shufrin and Eisenberger 2005)	1.9550	1.9550	1.0567
		Present theory (2D)	1.9534	1.9534	1.0564
		2D HSDT (Thai and Vo 2013)	1.9651	1.9651	1.0586
		Present theory (Quasi-3D)	2.008*	2.008[x]	1.1617
1.5	0.1	FSDT (Shufrin and Eisenberger 2005)	4.0250	2.0048	1.3879
		2D TSDT (Shufrin and Eisenberger 2005)	4.0253	2.0048	1.3879
		Present theory (2D)	4.0257	2.0049	1.3880
		2D HSDT (Thai and Vo 2013)	4.0258	2.0049	1.3880
		Present theory (Quasi-3D)	4.1154*	2.0305	1.4057
	0.2	FSDT (Shufrin and Eisenberger 2005)	3.3048	1.7941	1.2421
		2D TSDT (Shufrin and Eisenberger 2005)	3.3077	1.7946	1.2424
		Present theory (2D)	3.3084	1.7948	1.2425
		2D HSDT (Thai and Vo 2013)	3.3096	1.7951	1.2427
		Present theory (Quasi-3D)	3.5264*	1.8677	1.2931

Table 8 Continued

a /*b*	*h*/*b*	Theories	Loading mode ($\gamma 1, \gamma 2$)		
			1(-1,0)	2(0,-1)	3(-1,-1)
1.5	0.3	FSDT (Shufrin and Eisenberger 2005)	2.5457	1.5267	1.0570
		2D TSDT (Shufrin and Eisenberger 2005)	2.5545	1.5285	1.0582
		Present theory (2D)	2.5551	1.5287	1.0583
		2D HSDT (Thai and Vo 2013)	2.5580	1.5295	1.0589
		Present theory (Quasi-3D)	2.8015*	1.6401	1.1354
	0.4	FSDT (Shufrin and Eisenberger 2005)	1.9196	1.2632	0.8745
		2D TSDT (Shufrin and Eisenberger 2005)	1.9421	1.2670	0.8772
		Present theory (2D)	1.9423	1.2671	0.8772
		2D HSDT (Thai and Vo 2013)	1.9473	1.2686	0.8783
		Present theory (Quasi-3D)	2.1189*	1.3873	0.9605
2	0.1	FSDT (Shufrin and Eisenberger 2005)	3.7865	1.5093	1.2074
		2D TSDT (Shufrin and Eisenberger 2005)	3.7866	1.5093	1.2075
		Present theory (2D)	3.7870	1.5094	1.2075
		2D HSDT (Thai and Vo 2013)	3.7869	1.5094	1.2075
		Present theory (Quasi-3D)	3.8527*	1.5273	1.2219
	0.2	FSDT (Shufrin and Eisenberger 2005)	3.2637	1.3694	1.0955
		2D TSDT (Shufrin and Eisenberger 2005)	3.2654	1.3697	1.0958
		Present theory (2D)	3.2661	1.3699	1.0959
		2D HSDT (Thai and Vo 2013)	3.2666	1.3700	1.0960
		Present theory (Quasi-3D)	3.4370*	1.4194	1.1356
	0.3	FSDT (Shufrin and Eisenberger 2005)	2.5726	1.1862	0.9490
		2D TSDT (Shufrin and Eisenberger 2005)	2.5839	1.1873	0.9498
		Present theory (2D)	2.5855	1.1875	0.9500
		2D HSDT (Thai and Thuc, 2013)	2.5882	1.1879	0.9503
		Present theory (Quasi-3D)	2.8393^{+}	1.2664	1.0131
	0.4	FSDT (Shufrin and Eisenberger 2005)	1.9034	0.9991	0.7992
		2D TSDT (Shufrin and Eisenberger 2005)	1.9230	1.0015	0.8012
		Present theory (2D)	1.9242	1.0016	0.8013
		2D HSDT (Thai and Vo 2013)	1.9292	1.0025	0.8020
		Present theory (Quasi-3D)	2.0784^{+}	1.0920	0.8736

*Critical buckling occurs at (m, n) = (2,1)
^{x}Critical buckling occurs at (m, n) = (1,2)
$^{+}$Critical buckling occurs at (m, n) = (3,1)

frequency. These findings are clearly shown in Fig. 6. Fig. 6(a) illustrates the evolution of $\bar{\omega}$ as a function of the power index (p) for rectangular thicklates (a/h = 5). The comparison is made between the present (2D and Quasi-3D) and the theories of Quasi-3D (Belabed *et al*. 2014) and 2D Thai and Vo (2013). It could be observed in Fig. 6(a) that the frequency $\bar{\omega}$ increases exponentially with the decrease of the power index. The P-FGMs ceramic plate is the most rigid, which gives an important reduction in the pace of $\bar{\omega}$ for the power index p ($p < 2$). Above this value, the shape of the natural frequency curve tends to stabilize as the plate becomes more ductile. In addition, the effect of the geometric ratio (a/h) of the P-FGM plate on the evolution of the natural frequency is shown in Fig. 6(b). It should be noted that the highest maximum values of the natural frequency are obtained for the ceramic plate. The increase in the latter is accentuated with the increase in the geometric ratio (a/h = 10), from which the frequency curve remains stable. The increase in the power index reduces the natural frequency of the P-FGMs plate.

3.3 Numerical examples and results of buckling analysis

The processing of the buckling response of P-FGMs Aluminium/Alumina (Al/Al_2O_3) plates subjected to an in-plane compression load (N_0) which depends on the loading mode (γ), is evaluated by eliminating the transverse

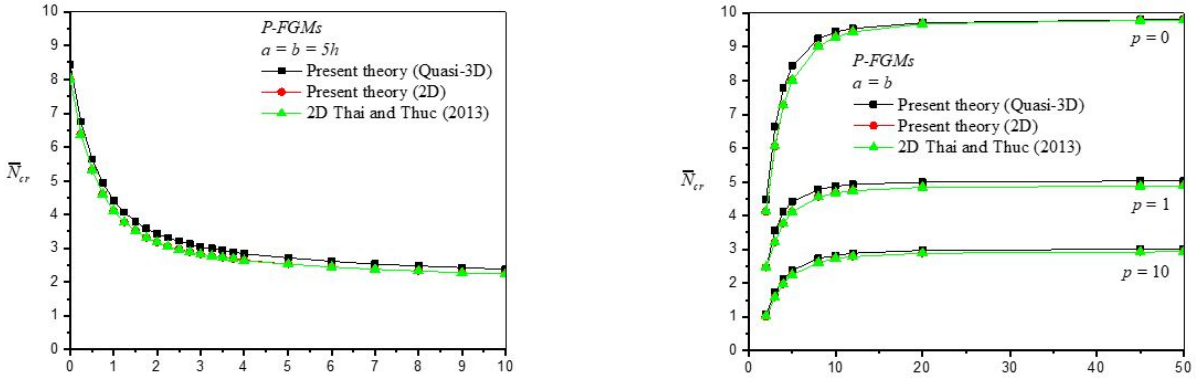

(a) p (b) a/h

Fig. 7 Comparison of the variation of non-dimensional critical buckling load $(\bar{N}_{cr})$ of plate under biaxial compression versus: (a) power law index (p); and (b) side-to-thickness ratio (a/h)

mechanical load (q) and kinetic energy.

Example 7. The reliability and the accuracy of the present theory in predicting the values of the critical buckling loads are highlighted in Table 8. Square and rectangular (a/b = 1, 1.5, 2), Al/Al_2O_3 homogeneous P-FGM thickplates (h/b = 0.1, 0.2, 0.3, 0.4), under various modes of in-plane compression loads ((γ_1, γ_2) = 1 (-1, 0), 2 (0, -1), 3 (-1, -1)). The critical load results $\bar{N}_{cr}$ are compared to the solutions of the theories FSDT and 2D HSDT of Shufrin and Eisenberger (2005) and 2D HSDT of Thai and Kim (2013). It should be noted that the present 2D theory is in good agreement with the two previous references and more particularly with the 2D HSDT results of Thai and Kim (2013), where the error rate is 0.595% which is not significant. As can be seen from all cases, the results obtained by the present quasi-3D HSDT theory are slightly over estimated. This is due to the presence of the stretching effect. Compared to the present theory in Quasi-3D and 2D with Thai and Kim (2013), the maximum error rate is 8.875% for $(a/b = 1,\ h/b = 0.4,\ \ (\gamma_1,\ \gamma_2) = (-1,\ -1))$, which is not significant either. It should be noted that, the values of $\bar{N}_{cr}$ increase simultaneously with the increase in the geometric ratio (a/b), the decrease in the ratio (h/b) and the loading modes for a square plate. It should be noted that the values of $\bar{N}_{cr}$ increase with the increase in the geometric ratio (a/b) and the decrease in both the ratio (h/b) and loading modes for a square plate.

Fig. 7 illustrates the variation of the critical buckling load $\bar{N}_{cr}$ as a function of the power index Eq. (7a) and the geometric ratio b/h Eq. (7b). From Fig. 7(a), it is obvious that the most important values of $\bar{N}_{cr}$ are found for most rigid square and thick P-FGM plates (a/h = 5). The increase in the critical buckling load depends strongly on the power index (p) when it is less than 2. Above this value the variation of $\bar{N}_{cr}$ is quasi weak. Fig. 7(b) shows the evolution of the critical load as a function of the (a/b) ratio for a square P-FGMs plate, for three power indices (p = 0, 1 and 10). The figure shows the comparison of the present 2D theory and Quasi-3D with 2D theory of Thai and Kim (2013). It should be observed that the largest curves corresponding to the largest values of the critical load are obtained for the lowest power index, they are of the order of 2 times and 3.2 times greater in comparison with the values obtained for the indices p = 1 and p = 10. With the exception of ceramic plates, there is always a small difference between the Quasi 3D and 2D HSDT results, where the Quasi-3D HSDT results are overestimated compared to 2D HSDT results. This is due to the thickness stretching effect, which is more important for the more ductile and thick plates.

4. Conclusions

A new 2D HSDT and Quasi-3D hybrid shear theory (polynomial-hyperbolic-exponential) to analyze bending, free vibration and buckling of P-FGMs, E-FGMs, and MT-FGMs plates with simply supported edges. The theoretical formulation begins with a displacement field with five unknowns, three of which are a transverse displacement of the membrane's bending, shearing and stretching of the plate thickness. The displacement due to the thickness stretching is developed by the transverse shear stress effect, satisfying the boundary conditions of zero stress on the free plate surfaces. The effects of several parameters such as the volume fraction index, the geometric ratios, the frequency modes, the mode parameters of in-plane compression load and the material properties, on the axial displacement, the deflection, the stresses, the natural frequencies and the buckling critical load are analyzed. The accuracy of the proposed model is verified by comparing its results with theories from the literature. This theory is found to be appropriate, simple and accurate, and among the results the following are drawn:

- The results obtained are in good agreement and closer to the different quasi-3D and 2D HSDT results in many cases, which shows the convergence of the theory.
- For the E-FGMs plates, the deflection $\bar{w}$ becomes more important with the decrease in the power index (p) and the geometric ratio (a/h) as well as the increase of the ratio (b/a). However, for the P-FGM, $\bar{w}$ increases with the increase of the index (p).

- For the P-FGM plates, $\bar{u}$ increases with the increase of the power index (p). However, $\bar{\sigma}_{xx}(z)$,$\bar{\beta}$ $\bar{\omega}$, , $\hat{\omega}$ et$\bar{N}_{cr}$ on the opposite increase with the decrease of the index (p).
- The decrease in the plate geometric ratio (a/h) leads to the reduction of the parameters $\bar{\beta}$ and $\hat{\omega}$. An inverse behaviour is noted for $\bar{\omega}$. This is due to the fact that the first two dimensionless parameters and the third dimensionless one are respectively proportional and inversely proportional to (a/h). Moreover, the increase in $\bar{\omega}$and $\hat{\omega}$ is influenced by the increase in the frequency modes.
- The shear stresses $\bar{\tau}_{xz}(z)$ are less important than $\bar{\sigma}_{xx}(z)$ and $\bar{\tau}_{xy}(z)$.
- The same behavior is observed for the two curves of $\bar{\omega}$ and $\bar{N}_{cr}$, and for all the modes of the in-plane compression load. The largest values of $\bar{\omega}$ and $\bar{N}_{cr}$ are obtained for thick and homogeneous plates.

Acknowledgments

The research reported herein was funded by the Deanship of Scientific Research at the University of Hail, Saudi Arabia, through the project number RG- 20098. The authors would like to express their deepest gratitude to the Deanship of Scientific Research and to the College of Engineering at the University of Hail for providing necessary support to conducting this research.

References

Abualnour, M., Houari, M.S.A., Tounsi, A. and Mahmoud, S.R. (2018), "A novel quasi-3D trigonometric plate theory for free vibration analysis of advanced composite plates", *Compos. Struct.*, **184**, 688-697. https://doi.org/10.1016/j.compstruct.2017.10.047

Atmane, H.A., Tounsi, A. and Mechab, I. (2010), "Free vibration analysis offunctionally graded plates resting on Winkler–Pasternak elastic foundations using a new shear deformation theory", *Int. J. Mech. Mater. Des.*, **6**(2), 113-121. https://doi.org/10.1007/s10999-010-9110-x

Ameur, M., Tounsi, A., Mechab, I. and El Bedia, A.A. (2011), "A new trigonometric shear deformation theory for bending analysis of functionally graded plates resting on elastic foundations", *KSCE J. Civil Eng.*, **15**(8), 1405-1414. https://doi.org/10.1007/s12205-011-1361-z

Amir, S., Arshid, E., Rasti-Alhosseini, S.A. and Loghman, A. (2020), "Quasi-3D tangential shear deformation theory for size-dependent free vibration analysis of three-layered FG porous micro rectangular plate integrated by nano-composite faces in hygrothermal environment", *J. Thermal Stress.*, **43**(2), 133-156. https://doi.org/10.1080/01495739.2019.1660601

Arani, A.G., Cheraghbak, A. and Kolahchi, R. (2016), "Dynamic buckling of FGM viscoelastic nano-plates resting on orthotropic elastic medium based on sinusoidal shear deformation theory", *Struct. Eng. Mech., Int. J.*, **60**(3), 489-505. https://doi.org/10.12989/sem.2016.60.3.489

Arefi, M. and Allam, M.N.M. (2015), "Nonlinear responses of an arbitrary FGP circular plate resting on the Winkler-Pasternak foundation", *Smart Struct., Syst., Int. J.*, **16**(1), 81-100. https://doi.org/10.12989/sss.2015.16.1.081

Aydogdu, M. (2009), "A new shear deformation theory for laminated composite plates", *Compos. Struct.*, **89**(1), 94-101. https://doi.org/10.1016/j.compstruct.2008.07.008

Baferani, A.H., Saidi, A.R. and Ehteshami, H. (2011), "Accurate solution for free vibration analysis of functionally graded thick rectangular plates resting on elastic foundation", *Compos. Struct.*, **93**, 1842-1853. https://doi.org/10.1016/j.compstruct.2011.01.020

Barati, M.R. and Shahverdi, H. (2016), "A four-variable plate theory for thermal vibration of embedded FG nanoplates under non-uniform temperature distributions with different boundary conditions", *Struct. Eng. Mech., Int. J.*, **60**(4), 707-727. https://doi.org/10.12989/sem.2016.60.4.707

Belabed, Z., Houari, M.S.A., Tounsi, A., Mahmoud, S.R. and Bég, O.A. (2014), "An efficient and simple higher order shear and normal deformation theory for functionally graded material (FGM) plates", *Compos. Part B Eng.*, **60**, 274-283. https://doi.org/10.1016/j.compositesb.2013.12.057

Beldjelili, Y., Tounsi, A. and Mahmoud, S.R. (2016), "Hygro-thermo-mechanical bending of S-FGM plates resting on variable elastic foundations using a four-variable trigonometric plate theory", *Smart Struct., Syst., Int. J.*, **18**(4), 755-786. https://doi.org/10.12989/sss.2016.18.4.755

Belkhodja, Y., Ouinas, D., Zaoui, F.Z. and Fekirini, H. (2019), "An exponential-trigonometric higher order shear deformation theory (HSDT) for bending, free vibration, and buckling analysis of functionally graded materials (FGMs) plates", *Adv. Compos. Lett.*, **28**, 1-19. https://doi.org/10.1177/0963693519875739

Benyoucef, S., Mechab, I., Tounsi, A., Fekrar, A. and Atmane, H.A. (2010), "Bending of thick functionally graded plates resting on Winkler–Pasternak elastic foundations", *Mech. Compos. Mater.*, **46**, 425-434. https://doi.org/10.1007/s11029-010-9159-5

Bouderba, B., Houari, M.S.A. and Tounsi, A. (2013), "Thermomechanical bending response of FGM thick plates resting on Winkler-Pasternak elastic foundations", *Steel Compos. Struct., Int. J.*, **14**(1), 85-104. https://doi.org/10.12989/scs.2013.14.1.085

Bourada, M., Tounsi, A., Houari, M.S.A. and Adda, B.E.A. (2012), "A new four-variable refined plate theory for thermal buckling analysis of functionally graded sandwich plates", *J. Sandw. Struct. Mater.*, **14**(1), 5-33. https://doi.org/10.1177%2F1099636211426386

Carrera, E., Brischetto, S. and Robaldo, A. (2008), "Variable kinematic model for the analysis of functionally graded material plates", *AIAA J.*, **46**(1), 194-203. https://doi.org/10.2514/1.32490

Carrera, E., Brischetto, S., Cinefra, M. and Soave, M. (2011), "Effects of thickness stretching in functionally graded plates and shells", *Compos. Part B*, **42**(2), 123-133. https://doi.org/10.1016/j.compositesb.2010.10.005

Celebi, K., Yarimpabuc, D. and Keles, I. (2016), "A unified method for stresses in FGM sphere with exponentially-varying properties", *Struct. Eng. Mech., Int. J.*, **57**(5), 823-835. https://doi.org/10.12989/sem.2016.57.5.823

Chen, Y.Z. (2018), "Transfer matrix method for solution of FGMs thick-walled cylinder with arbitrary inhomogeneous elastic response", *Smart Struct. Syst., Int. J.*, **21**(4), 469-477. https://doi.org/10.12989/sss.2018.21.4.469

Chikh, A., Tounsi, A., Hebali, H. and Mahmoud, S.R. (2017), "Thermal buckling analysis of cross-ply laminated plates using a simplified HSDT", *Smart Struct. Syst., Int. J.*, **19**(3), 289-297. https://doi.org/10.12989/sss.2017.19.3.289

Daikh, A.A. and Zenkour, A.M. (2019), "Effect of porosity on the bending analysis of various functionally graded sandwich plates", *Mater. Res. Express*, **6**(6), 065703.

https://doi.org/10.1088/2053-1591/ab0971
Darabi, A. and Vosoughi, A.R. (2016), "Hybrid inverse method for small scale parameter estimation of FG nanobeams", *Steel Compos. Struct.*, *Int. J.*, **20**(5), 1119-1131. https://doi.org/10.12989/scs.2016.20.5.1119
Ebrahimi, F. and Daman, M. (2017), "Nonlocal thermo-electro-mechanical vibration analysis of smart curved FG piezoelectric Timoshenko nanobeam", *Smart Struct. Syst.*, *Int. J.*, **20**(3), 351-368. https://doi.org/10.12989/sss.2017.20.3.351
Ferreira, A.J.M., Batra, R.C., Roque, C.M.C., Qian, L.F. and Martins, P.A.L.S. (2005), "Static analysis of functionally graded plates using third-order shear deformation theory", *Compos. Struct.*, **69**, 449-457. https://doi.org/10.1016/j.compstruct.2004.08.003
Fukui, Y. (1991), "Fundamental investigation of functionally gradient material manufacturing system using centrifugal force", *JSME Int. J. Ser.* 3, Vib., *Control Eng.*, *Eng.*, *Ind.*, **34**(1), 144-148. https://doi.org/10.1299/jsmec1988.34.144
Fukushima, T., Kuroda, S. and Kitahara, S. (1990), "Gradient coatings formed by plasma twin torches and those properties", *Proceedings of the First International Symposium on Functionally Gradient Materials*, Tokyo, Japan, pp. 145-150.
Ghugal, Y.M. and Sayyad, A.S. (2010), "A static flexure of thick isotropic plates using trigonometric shear deformation theory", *J. Solid Mech.*, **2**(1), 79-90.
Guerroudj, H.Z., Yeghnem, R., Kaci, A., Zaoui, F.Z., Benyoucef, S. and Tounsi, A. (2018), "Eigenfrequencies of advanced composite plates using an efficient hybrid quasi-3D shear deformation theory", *Smart Struct. Syst.*, *Int. J.*, **22**(1), 121-132. https://doi.org/10.12989/sss.2018.22.1.121
Hanifi, H.A.L., Kaci, A. and Tounsi, A. (2017), "On the size-dependent behavior of functionally graded micro-beams with porosities", *Struct. Eng. Mech.*, *Int. J.*, **64**(5), 527-541. https://doi.org/10.12989/scs.2017.64.5.527
Hebali, H., Tounsi, A., Houari, M.S.A., Bessaim, A. and Bedia, E.A.A. (2014), "New quasi-3D hyperbolic shear deformation theory for the static and free vibration analysis of functionally graded plates", (*ASCE*). *J. Eng. Mech.*, **140**(2), 374-383. https://doi.org/10.1061/(ASCE)EM.1943-7889.0000665
Hebbar, N., Hebbar, I., Ouinas D. and Bourada, M. (2020), "Numerical modeling of bending, buckling, and vibration of functionally graded beams by using a higher-order shear deformation theory", *Frattura ed Integrità Strutturale*, **14**(52), 230-246. https://doi.org/10.3221/IGF-ESIS.52.18
Hosseini-Hashemi, S., Fadaee, M. and Atashipour, S.R. (2011a), "Study on the free vibration of thick functionally graded rectangular plates according to a new exact closed form procedure", *Compos. Struct.*, **93**(2), 722-735. https://doi.org/10.1016/j.compstruct.2010.08.007
Hosseini-Hashemi, S., Fadaee, M. and Atashipour, S.R. (2011b), "A new exact analytical approach for free vibration of Reissner–Mindlin functionally graded rectangular plates", *Int. J. Mech. Sci.*, **53**(1), 11-22. https://doi.org/10.1016/j.ijmecsci.2010.10.002
Hosseini-Hashemi, S., Salehipour, H. and Atashipour, S.R. (2012), "Exact three-dimensional free vibration analysis of thick homogeneous plates coated by a functionally graded layer", *Acta Mech.*, **223**, 2153-2166. https://doi.org/10.1007/s00707-012-0683-3
Iurlaro, L., Gherlone, M. and Di Sciuva, M. (2014), "Bending and free vibration analysis of functionally graded sandwich plates using the Refined Zigzag theory", *J Sandw. Struct. Mater.*, **16**(6), 669-699. https://doi.org/10.1177/1099636214548618
Jha, D.K., Tarun, K. and Singh, R.K. (2012), "Higher order shear and normal deformation theory for natural frequency of functionally graded rectangular plates", *Nucl. Eng. Des.*, **250**, 8-13. https://doi.org/10.1016/j.nucengdes.2012.05.001
Kar, V.R. and Panda, S.K. (2016a), "Post-buckling behaviour of shear deformable functionally graded curved shell panel under edge compression", *Int. J. Mech. Sci.*, **115-116**, 318-324. https://doi.org/10.1016/j.ijmecsci.2016.07.014
Kar, V.R. and Panda, S.K. (2016b), "Geometrical nonlinear free vibration analysis of FGM spherical panel under nonlinear thermal loading with TD and TID properties", *J. Therm. Stress.*, **39**(8), 942-959. https://doi.org/10.1080/01495739.2016.1188623
Kawasaki, A. and Watanabe, R. (1988), "Powder metallurgical fabrication of the thermal-stress relief type of functionally gradient materials", *Sintering'87*, London, UK, Volume 2, pp. 1197-1202.
Kiran, M.C. and Kattimani, S.C. (2018), "Free vibration and static analysis of functionally graded skew magneto-electro-elastic plate", *Smart Struct. Syst.*, *Int. J.*, **21**(4), 493-519. https://doi.org/10.12989/sss.2018.21.4.493
Koizumi, M. (1997), "FGM activities in Japan", *Compos. Part B*, **28**(1-2), 1-4. https://doi.org/10.1016/S1359-8368(96)00016-9
Kolahchi, R., Safari, M. and Esmailpour, M. (2016), "Dynamic stability analysis of temperature-dependent functionally graded CNT-reinforced visco-plates resting on orthotropic elastomeric medium", *Compos. Struct.*, **150**, 255-265. https://doi.org/10.1016/j.compstruct.2016.05.023
Kolahchi, R., Zarei, M.S., Hajmohammad, M.H. and Oskouei, A.N. (2017), "Visco-nonlocal-refined Zigzag theories for dynamic buckling of laminated nanoplates using differential cubature-Bolotin methods", *Thin-Wall. Struct.*, **113**, 162-169. https://doi.org/10.1016/j.tws.2017.01.016
Lal, R. and Saini, R. (2020), "Vibration analysis of FGM circular plates under non-linear temperature variation using generalized differential quadrature rule", *Appl. Acoustics*, **158**, 107027. https://doi.org/10.1016/j.apacoust.2019.107027
Le, C.I., Pham, V.N. and Nguyen, D.K. (2020), "Free vibration of FGSW plates partially supported by Pasternak foundation based on refined shear deformation theories", *Math. Problems Eng.*, 13 p. https://doi.org/10.1155/2020/7180453
Madani, H., Hosseini, H. and Shokravi, M. (2016), "Differential cubature method for vibration analysis of embedded FG-CNT-reinforced piezoelectric cylindrical shells subjected to uniform and non-uniform temperature distributions", *Steel Compos. Struct.*, *Int. J.*, **22**(4), 889-913. https://doi.org/10.12989/scs.2016.22.4.889
Mahesh, V., Kattimani, S., Harursampath, D. and Trung, N.T. (2019), "Coupled evaluation of the free vibration characteristics of magneto-electro-elastic skew plates in hygrothermal environment", *Smart Struct. Syst.*, *Int. J.*, **24**(2), 267-292. https://doi.org/10.12989/sss.2019.24.2.267
Mantari, J.L. and Soares, C.G. (2012a), "Bending analysis of thick exponentially graded plates using a new trigonometric higher order shear deformation theory", *Compos. Struct.*, **94**(6), 1991-2000. https://doi.org/10.1016/j.compstruct.2012.01.005
Mantari, J.L. and Soares, C.G. (2012b), "Generalized hybrid quasi-3D shear deformation theory for the static analysis of advanced composite plates", *Compos. Struct.*, **94**(8), 2561-2575. https://doi.org/10.1016/j.compstruct.2012.02.019
Mantari, J.L. and Soares, C.G. (2013), "A novel higher-order shear deformation theory with stretching effect for functionally graded plates", *Compos. Part B*, **45**(1), 268-281. https://doi.org/10.1016/j.compositesb.2012.05.036
Mantari, J.L. and Soares, C.G. (2014), "Optimized sinusoidal higher order shear deformation theory for the analysis of functionally graded plates and shell", *Compos. Part B*, **56**, 126-136. https://doi.org/10.1016/j.compositesb.2013.07.027
Mantari, J.L., Oktem, A.S. and Soares, C.G. (2012), "Bending response of functionally graded plates by using a new higher order shear deformation theory", *Compos. Struct.*, **94**(2), 714-723. https://doi.org/10.1016/j.compstruct.2011.09.007

Matsunaga, H. (2008), "Free vibration and stability of functionally graded plates according to a 2-D higher-order deformation theory", *Compos. Struct.*, **82**(4), 499-512. https://doi.org/10.1016/j.compstruct.2007.01.030

Meftah, A., Bakora, A., Zaoui, F.Z., Tounsi, A. and Adda Bedia, E.A. (2017), "A non-polynomial four variable refined plate theory for free vibration of functionally graded thick rectangular plates on elastic foundation", *Steel Compos. Struct., Int. J.*, **23**(3), 317-330. https://doi.org/10.12989/scs.2017.23.3.317

Miyamoto, Y., Nakanishi, H., Tanaka, I., Okamoto, T. and Yamada, O. (1990), "Gas pressure combustion sintering of TiC-Ni FGM", *Proceedings of the First International Symposium, FGM*, Tokyo, Japan, pp. 257-262.

Mohammadimehr, M. and Alimirzaei, S. (2017), "Buckling and free vibration analysis of tapered FG-CNTRC micro Reddy beam under longitudinal magnetic field using FEM", *Smart Struct. Syst., Int. J.*, **19**(3), 309-322. https://doi.org/10.12989/sss.2017.19.3.309

Neves, A.M.A., Ferreira, A.J.M., Carrera, E., Roque, C.M.C., Cinefra, M., Jorge, R.M.N. and Soares, C.M.M. (2011), "Bending of FGM plates by a sinusoidal plate formulation and collocation with radial basis functions", *Mech. Res. Commun.*, **38**(5), 368-371. https://doi.org/10.1016/j.mechrescom.2011.04.011

Neves, A.M.A., Ferreira, A.J.M., Carrera, E., Roque, C.M.C., Cinefra, M., Jorge, R.M.N. and Soares, C.M.M. (2012a), "A quasi-3D sinusoidal shear deformation theory for the static and free vibration analysis of functionally graded plates", *Compos. Part B Eng.*, **43**(2), 711-725. https://doi.org/10.1016/j.compositesb.2011.08.009

Neves, A.M.A., Ferreira, A.J.M., Carrera, E., Cinefra, M., Roque, C.M.C., Jorge, R.M.N. and Soares, C.M.M. (2012b), "A quasi-3D hyperbolic shear deformation theory for the static and free vibration analysis of functionally graded plates", *Compos. Struct.*, **94**(5), 1814-1825. https://doi.org/10.1016/j.compstruct.2011.12.005

Neves, A.M.A., Ferreira, A.J.M., Carrera, E., Cinefra, M., Roque, C.M.C., Jorge, R.M.N. and Soares, C.M. (2013), "Static, free vibration and buckling analysis of isotropic and sandwich functionally graded plates using a quasi-3D higher-order shear deformation theory and a meshless technique", *Compos. Part B*, **44**(1), 657-674. https://doi.org/10.1016/j.compositesb.2012.01.089

Nguyen, T.K. (2014), "A higher-order hyperbolic shear deformation plate model for analysis of functionally graded materials", *Int. J. Mech. Mater. Des.*, **11**(2), 203-219. https://doi.org/10.1007/s10999-014-9260-3

Niino, A. and Maeda, S. (1990), "Recent development status of functionally gradient materials", *ISIJ Int.*, **30**(9), 699-703. https://doi.org/10.2355/isijinternational.30.699

Qian, L.F., Batra, R.C. and Chen, L.M. (2004), "Static and dynamic deformations of thick functionally graded elastic plates by using higher-order shear and normal deformable plate theory and meshless local Petrov–Galerkin method", *Compos. Part B*, **35**(6-8), 685-697. https://doi.org/10.1016/j.compositesb.2004.02.004

Raminnea, M., Biglari, H. and Tahami, F.V. (2016), "Nonlinear higher order Reddy theory for temperaturedependent vibration and instability of embedded functionally graded pipes conveying fluid-nanoparticle mixture", *Struct. Eng. Mech., Int. J.*, **59**(1), 153-186. https://doi.org/10.12989/sem.2016.59.1.153

Reddy, J.N. (2000), "Analysis of functionally graded plates", *Int. J. Numer. Methods Eng.*, **47**(1-3), 663-684. https://doi.org/10.1002/(SICI)1097-0207(20000110/30)47:1/3<663::AID-NME787>3.0.CO; 2-8

Sasaki, M., Wang, Y., Hirano, T. and Hirai, T. (1989), "Design of SiC/C functionally gradient material and its preparation by chemical vapor deposition", *J. Ceram. Soc. Japan*, **97**(1125), 539-543. https://doi.org/10.2109/jcersj.97.539

Sata, N., Sanada, N., Hirano, T. and Niino, M. (1990), "Fabrication of a functionally gradient material by using a self-propagating reaction process", *Proceedings of the First Int. Symp. On Combustion and Plasma Synthesis of High-Temperature Materials*, pp. 195-203.

Shimoda, N., Kitaguchi, S., Saito, T., Takigawa, H. and Koga, M. (1990), "Production of functionally gradient materials by applying low pressure plasma spray", *Proceedings of the First International Symposium on Funtionally Gradient Materials*, Sendai, Tokyo, Japan, pp. 151-156.

Shokravi, M. and Jalili, N. (2017), "Dynamic buckling response of temperature-dependent functionally graded-carbon nanotubes-reinforced sandwich microplates considering structural damping", *Smart Struct. Syst., Int. J.*, **20**(5), 583-593. https://doi.org/10.12989/sss.2017.20.5.583

Shufrin, I. and Eisenberger, M. (2005), "Stability and vibration of shear deformable plates-first order and higher order analyses", *Int. J. Solids Struct.* **42**(3-4), 1225-1251. https://doi.org/10.1016/j.ijsolstr.2004.06.067

Singh, V.K. and Panda, S.K. (2015), "Large amplitude free vibration analysis of laminated composite spherical shells embedded with piezoelectric layers", *Smart Struct. Syst., Int. J.*, **16**(5), 853-872. https://doi.org/10.12989/sss.2015.16.5.853

Talha, M. and Singh, B.N. (2010), "Static response and free vibration analysis of FGM plates using higher order shear deformation theory", *Appl. Math. Modell.*, **34**(12), 3991-4011. https://doi.org/10.1016/j.apm.2010.03.034

Thai, H.T. and Kim, S.E. (2013), "A simple higher-order shear deformation theory for bending and free vibration analysis of functionally graded plates", *Compos. Struct.*, **96**, 165-173. https://doi.org/10.1016/j.compstruct.2012.08.025

Thai, H.T. and Vo, T.P. (2013), "A new sinusoidal shear deformation theory for bending, buckling, and vibration of functionally graded plates", *Applied Math. Modell.*, **37**(5), 3269-3281. https://doi.org/10.1016/j.apm.2012.08.008

Tornabene, F. (2009), "Free vibration analysis of functionally graded conical, cylindrical shell and annular plate structures with a four-parameter power-law distribution", *Comput. Meth. Appl. Mech. Eng.*, **198**(37-40), 2911-2935. https://doi.org/10.1016/j.cma.2009.04.011

Trinh, T.H., Nguyen, D.K., Gan, B.S. and Alexandrov, S. (2016), "Post-buckling responses of elastoplastic FGM beams on nonlinear elastic foundation", *Struct. Eng. Mech., Int. J.*, **58**(3), 515-532. https://doi.org/10.12989/sem.2016.58.3.515

Vaghefi, R., Baradaran, G.H. and Koohkan, H. (2010), "Three-dimensional static analysis of thick functionally graded plates by using meshless local Petrov – Galerkin (MLPG) method", *Eng. Anal. Bound. Elem.*, **34**(6), 564-573. https://doi.org/10.1016/j.enganabound.2010.01.005

Vel, S.S. and Batra, R.C. (2004), "Three-dimensional exact solution for the vibration of functionally graded rectangular plates", *J. Sound Vib.*, **272**(3-5), 703-730. https://doi.org/10.1016/S0022-460X(03)00412-7

Wu, C.P. and Li, H.Y. (2010), "An RMVT-based third-order shear deformation theory of multilayered functionally graded material plates", *Compos. Struct.*, **92**(10), 2591-2605. https://doi.org/10.1016/j.compstruct.2010.01.022

Wu, C.P., Chiu, K.H. and Wang, Y.M. (2011), "RMVT-based meshless collocation and element free Galerkin methods for the quasi-3D analysis of multilayered composite and FGM plates", *Compos. Struct.*, **93**(2), 923-943. https://doi.org/10.1016/j.compstruct.2010.11.015

Xiang, S. and Kang, G.W. (2013), "A nth-order shear deformation theory for the bending analysis on the functionally graded plates", *Eur. J. Mech. A/Solids*, **37**, 336-343.

https://doi.org/10.1016/j.euromechsol.2012.08.005
Xiang, S., Kang, G.W., Yang, M.S. and Zhao, Y. (2013), "Natural frequencies of sandwich plate with functionally graded face and homogeneous core", *Compos. Struct.*, **96**, 226-231. https://doi.org/10.1016/j.compstruct.2012.09.003
Younsi, A., Tounsi, A., Zaoui, F.Z., Bousahla, A.A. and Mahmoud S.R. (2018), "Novel quasi-3D and 2D shear deformation theories for bending and free vibration analysis of FGM plates", *Geomech. Eng., Int. J.*, **14**(6), 519-532. https://doi.org/10.12989/gae.2018.14.6.519
Yuki, M., Murayama, T., Irisawa, T., Kawasaki, A. and Watanabe, R. (1990), "FGM'90", *Proceedings of the 1st International Symposium on Functionally Gradient Materials*, Sendai, FGM Forum, Tokyo, Japan, pp. 203-208.
Zafarmand, H. and Kadkhodayan, M. (2015), "Three dimensional elasticity solution for static and dynamic analysis of multi-directional functionally graded thick sector plates with general boundary conditions", *Compos. Part B*, **69**, 592-602. https://doi.org/10.1016/j.compositesb.2014.10.048
Zaoui, F.Z., Tounsi, A. and Ouinas, D. (2017), "Free vibration of functionally graded plates resting on elastic foundations based on quasi-3D hybrid-type higher order shear deformation theory", *Smart Struct. Syst., Int. J.*, **20**(4), 509-524. https://doi.org/10.12989/sss.2017.20.4.509
Zaoui, F.Z., Ouinas, D. and Tounsi, A. (2019), "New 2D and quasi-3D shear deformation theories for free vibration of functionally graded plates on elastic foundations", *Compos. Part B*, **159**, 231-247. https://doi.org/10.1016/j.compositesb.2018.09.051
Zaoui, F.Z., Tounsi, A., Ouinas, D. and Olay, J.A.V. (2020), "A refined HSDT for bending and dynamic analysis of FGM plates", *Struct. Eng. Mech., Int. J.*, **74**(1), 105-119. https://doi.org/10.12989/sem.2020.74.1.105
Zenkour, A.M. (2006), "Generalized shear deformation theory for bending analysis of functionally graded plates", *Appl. Math. Model.*, **30**(1), 67-84. https://doi.org/10.1016/j.apm.2005.03.009
Zenkour, A.M. (2007), "Benchmark trigonometric and 3-D elasticity solutions for an exponentially graded thick rectangular plate", *Arch. Appl. Mech.*, **77**(4), 197-214. https://doi.org/10.1007/s00419-006-0084-y
Zenkour, A.M. (2009), "The refined sinusoidal theory for FGM plates on elastic foundations", *Int. J. Mech. Sci.*, **51**(11-12), 869-880. https://doi.org/10.1016/j.ijmecsci.2009.09.026
Zhang, H., Jiang, J.K. and Zhang, Z.C. (2014), "Threedimensional elasticity solutions for bending of generally supported thick functionally graded plates", *Appl. Math. Mech.*, **35**(11), 1467-1478. https://doi.org/10.1007/s10483-014-1871-7
Zhou, D., Cheung, Y.K., Au, F.T.K. and Lo, S.H. (2002), "Threedimensional vibration analysis of thick rectangular plates using Chebyshev polynomial and Ritz method", *Int. J. Solids Struct.*, **39**, 6339-6353. https://doi.org/10.1016/S0020-7683(02)00460-2
Zidi, M., Tounsi, A., Houari, M.S.A., Adda Bedia, E.A. and Anwar Bég, O. (2014), "Bending analysis of FGM plates under hygro-thermo-mechanical loading using a four variable refined plate theory", *Aerosp. Sci. Technol.*, **34**, 24-34. https://doi.org/10.1016/j.ast.2014.02.001